REVIEWS OF MODERN PHYSICS, VOLUME 78, JANUARY 2006

Dynamics of Bose-Einstein condensates in optical lattices

Oliver Morsch*

Dipartimento di Fisica "Enrico Fermi," CNR-INFM, Largo Pontecorvo 3, I-56127 Pisa, Italy

Markus Oberthaler†

Kirchhoff Institut für Physik, Universität Heidelberg, Im Neuenheimer Feld 227, D-69120 Heidelberg, Germany

(Published 27 February 2006)

Matter waves inside periodic potentials are well known from solid-state physics, where electrons interacting with a crystal lattice are considered. Atomic Bose-Einstein condensates inside light-induced periodic potentials (optical lattices) share many features with electrons in solids, but also with light waves in nonlinear materials and other nonlinear systems. Generally, atom-atom interactions in Bose-Einstein condensates lead to rich and interesting nonlinear effects. Furthermore, the experimental control over the parameters of the periodic potential and the condensate make it possible to enter regimes inaccessible in other systems. In this review, an introduction to the physics of ultracold bosonic atoms in optical lattices is given and an overview of the theoretical and experimental advances to date.

DOI: 10.1103/RevModPhys.78.179 PACS number(s): 03.75.Lm, 42.50.Vk, 05.45.−a

CONTENTS

*Electronic address: morsch@df.unipi.it
†Electronic address: markus.oberthaler@kip.uni-heidelberg.de

I. INTRODUCTION

The 1980s and 1990s saw two major breakthroughs in atomic physics. Two Nobel prizes were awarded for these achievements: for laser cooling of atoms in 1997 (Chu, 1998; Cohen-Tannoudji, 1998; Phillips, 1998) and for Bose-Einstein condensation (BEC) in 2001 (Cornell and Wieman, 2002; Ketterle, 2002). Laser cooling led to record low temperatures in the micro-Kelvin regime and, among other things, to the realization of artificial crystals bound by light, so-called optical lattices. It also paved the way for even more powerful cooling techniques, in particular evaporative cooling, which made possible the Bose-Einstein condensation of a dilute gas of alkali atoms in 1995.[1] In this review, we shall take a closer look at the merger of these two fields: optical lattices and Bose-Einstein condensates. Shortly after the first realization of BEC, a number of research groups started investigating the properties of BECs in periodic potentials, often preceded and sometimes followed by theoretical efforts. Nearly ten years on, BECs in optical lattices have matured into an active field of research in its own right, which means that, on the one hand, it is exciting and thriving and holds a lot of promise for future developments. On the other hand, the amount of literature on the subject has reached dimensions that make it difficult for a newcomer to get a systematic overview on what has been done thus far and what remains to be done in the future. The present paper aims to provide exactly that.

Apart from being a marriage of two very recent disciplines within atomic and laser physics, BECs in optical lattices have relatives in many other fields of physics. One obvious connection is that with condensed matter physics: electrons in crystal lattices[2] bear more than a passing resemblance to the subject of this paper, and a large amount of theoretical and experimental work on, for instance, the Bose-Hubbard model and the Mott insulator transition, has dealt with this analogy. The amount of literature on this system alone is so large that we refer the interested reader to more specialized reviews[3] (Bloch, 2005; Jaksch and Zoller, 2005). In the present paper we shall, however, focus our attention on another interesting analogy, namely, that with nonlinear optics and nonlinear physics in general. We shall, therefore, present in some detail the theoretical treatment of the *dynamics* of condensates in periodic potentials. As the atoms in a BEC can, in some cases, interact with each other rather strongly through collisions, nonlinearities can play an important role in the behavior of the system. This link with nonlinear optics can, we believe, in future lead to useful exchanges.

The aim of this review is to satisfy the needs both of newcomers and of experts in the field. As these two aims are not easy to achieve at the same time, we have opted for a two-part approach. In order to cater to the needs of newcomers, we devote Sec. II of this paper to a tutorial-style introduction to the history, methods, and main research motivations concerning optical lattices, Bose-Einstein condensates, and the combination of these two phenomena. A reader entirely new to the field should be able get a good overview from this part. Next, in Secs. III–V we present a systematic and comprehensive account of the theoretical treatment of Bose-Einstein condensates in periodic potentials. Section VI discusses the experiments carried out to date and links them to the theoretical work presented in the preceding sections. Finally, in Sec. VII we present some current trends and speculate on possible research directions for the future.

II. A TUTORIAL OVERVIEW

With hindsight, the idea of taking a Bose-Einstein condensate and combining it with the periodic potential of an optical lattice[4] may seem perfectly obvious, seeing as both of these experimental techniques were well established by the late 1990s. Moreover, by that time a number of theoretical papers had been published pointing out the intriguing phenomena that could probably be observed in such a system. The versatility and vast potential for doing interesting physics with BECs in lattices, though, only became clear once some of the theoretical proposals were actually tested in the laboratory. Since then, the field has progressed in leaps and bounds. In this part of our review, we want to give the reader a taste of what BECs and optical lattices are, how the subject of BECs in lattices was born, and how the system is actually realized in the lab. Finally, we give a motivation for studying this particular physical system. In this way, we pave the way for a more in-depth discussion.

A. From laser cooling to BEC

The first proposals for cooling atoms with laser light[5] were made when the laser itself was still in its infancy. As early as 1970, it was suggested that the Doppler ef-

[1]For theoretical and experimental reviews, see Dalfovo *et al.* (1999) and Leggett (2001) and Ketterle *et al.* (1999), respectively. Textbook-style monographs are Pethick and Smith (2000); Pitaevskii and Stringari (2003).
[2]For an introduction, see, e.g., Kittel (1996).
[3]For a popular account, see Bloch (2004).
[4]For reviews on optical lattices, see, e.g., Jessen and Deutsch (1996); Meacher (1998); Grynberg and Robilliard (2001).
[5]See Metcalf and van der Straten (1999) for a comprehensive introduction.

fect due to the thermal motion of atoms could be exploited in order to make them absorb laser light at a different rate depending on whether they moved away from or toward the laser. The net momentum kick felt by the atom could then be used to slow down an atomic beam or, if the light came from all spatial directions, to cool a gas of atoms. When this simple principle was finally applied in the early 1980s, it immediately led to unprecedentedly low temperatures only a few hundreds of micro-Kelvins above absolute zero. These temperatures were even lower than the researchers had hoped for because (previously neglected) optical pumping forces led to sub-Doppler cooling mechanisms. It was also soon realized that the spatial interference pattern created by the laser beams used for cooling effectively represented a three-dimensional egg carton for the atoms. Experiments confirmed the suspicion that one was, indeed, able to create artificial crystals bound by light. While initially near-resonant lattices were used in which atoms continuously scattered photons (leading to the cooling force), later studies were done with far-resonant conservative potentials. It is the latter kind of optical lattices that we shall deal with in this review.

Laser cooling of atoms soon became a versatile tool in atomic physics, with applications ranging from precision spectroscopy to atomic clocks and atom interferometers. Ultracold atoms also turned out to be an ideal raw material for the realization of magnetic traps for neutral atoms. Held in place by magnetic dipole forces, such atomic gases can then be evaporatively cooled by successively lowering the trap depth, thus letting the most energetic atoms escape and allowing the remaining ones to rethermalize. In this way, the fundamental limitations of laser cooling due to photon scattering can be overcome and temperatures as low as a few nano-Kelvins can be reached. If at the same time the density of the trapped gas is large enough, the phase-space density condition for Bose-Einstein condensation can be satisfied: a BEC is created.

Inspired by a paper on photon statistics by Satyendra Nath Bose, in 1926 Einstein predicted this new kind of phase transition in identical bosons when their phase space density exceeds unity. In that case, a macroscopic occupation of the lowest quantum level of the system occurs. The resulting Bose-Einstein condensate can be represented by a single order parameter, the macroscopic wave function ψ. Despite the discovery of several phenomena that could be explained by invoking the concept of Bose-Einstein condensation, notably superfluidity, it was only in 1995 that BEC was observed for the first time in its "ideal" form in a cloud of cold alkali atoms.[6]

Once the first Bose-Einstein condensates had been created, a flurry of experimental and theoretical activities started. Within a few years, the most important characteristics of BECs were measured and explained. Today, in a typical BEC experiment the protocol used is very similar to that of the first demonstrations:

(i) Atoms are cooled and collected in a magneto-optical trap (MOT).

(ii) The cold atom cloud is transferred into a conservative trap (either magnetic or optical).

(iii) By lowering the trap depth, forced evaporative cooling is achieved.

At the end of the evaporative cooling cycle, condensates with up to 10^7 atoms are now routinely created with alkali atoms. Although Bose-Einstein condensation has been achieved with a considerable number of atomic species, most of the experiments described in this review were carried out using BECs of rubidium (Rb) and sodium (Na). It is very likely, though, that in future experiments with optical lattices BECs of cesium, lithium, and other elements will be used too.[7] For the purposes of this review, the details of a typical experimental BEC setup are not crucial, and we refer the reader to the technical accounts published in the literature (Ketterle *et al.*, 1999).

Once a Bose-Einstein condensate has been created by evaporative cooling in a harmonic trap, the next logical step is to look at it and probe its properties. This can be done either *in situ*, i.e., with the condensate inside the trap, or using a time-of-flight technique. Although *in situ* diagnostics are a valuable tool for some applications, we shall concentrate here on the time-of-flight technique, which is very versatile and is also directly applicable to condensates in periodic potentials (see Sec. VI.A). This method consists in simply switching off the trapping field (magnetic or optical) at time $t=0$ and taking an image of the BEC a few (typically 5 to 25) milliseconds later. The image is most often taken by absorption, i.e., shining a resonant laser beam onto the atomic cloud and observing with a CCD camera the shadow cast by the absorption of photons. This and other methods, notably phase contrast imaging, are described in detail in Ketterle *et al.* (1999).

B. Optical lattices

In order to trap a Bose-Einstein condensate in a periodic rather than a harmonic potential, it is sufficient to exploit the interference pattern created by two or more overlapping laser beams and the light force exerted on the condensate atoms. In the following, we shall briefly remind the reader of the basic notions associated with the interaction between atoms and laser light and then proceed to explain the techniques used to create and manipulate optical lattices.

[6]A good account of the early BEC experiments and the relevant references can be found in Ketterle *et al.* (1999).

[7]Another interesting line of research has been opened up by ultracold fermions, which we shall briefly discuss in Sec. VII.B.

1. Light forces

Optical lattices and other optical traps (also called dipole force traps or simply dipole traps[8]) work on the principle of the ac Stark shift. When an atom is placed in a light field, the oscillating electric field of the latter induces an electric dipole moment in the atom. The interaction between this induced dipole and the electric field leads to an energy shift ΔE of an atomic energy level equal to

$$\Delta E = -\frac{1}{2}\alpha(\omega)\langle E^2(t)\rangle, \tag{1}$$

where $\alpha(\omega)$ with $\omega=\omega_{\rm res}+\Delta$ is the dynamic polarizability of the atomic level exhibiting a resonance at $\omega_{\rm res}$, Δ is the detuning of the light field from the atomic resonance, and the brackets $\langle\ \rangle$ denote a cycle average.

If the frequency of the light field is smaller than the atomic resonance frequency, i.e., $\Delta<0$ ("red-detuned"), the induced dipole $D=\alpha(\omega)E$ will be in phase with the electric field. Therefore, the resulting potential energy will be such that its gradient, which results in a force on the atom, points in the direction of increasing field. A stable optical trap can then be realized by simply focusing a laser beam to a waist of size w. If the cross section of the beam is Gaussian, the resulting position-dependent ac Stark shift [and hence the atom's potential energy $V(r,z)$]

$$\Delta E(r,z) = V(r,z) = V_0 \exp\left(-\frac{2r^2}{w[z]^2}\right), \tag{2}$$

$$w[z] = w_0\sqrt{1+\left(\frac{z}{z_R}\right)^2}, \tag{3}$$

where $V_0 \propto I_p/\Delta$ is the trap depth, with I_p the peak intensity of the beam, and w_0 and $z_R=w_0^2\pi/\lambda_L$ are the spot size (waist) and Rayleigh length, respectively, of the Gaussian beam. Expanding this expression at the waist (i.e., $z=0$) around $r=0$, we find that in the harmonic approximation the radial oscillation frequency (i.e., perpendicular to the propagation direction of the beam) of an atom of mass m in such a potential is given by

$$\omega_\perp = \frac{1}{w}\sqrt{\frac{2V_0}{m}}. \tag{4}$$

The depth V_0 of an optical trap scales as I_p/Δ, whereas the rate Γ at which atoms at the center of the trap will spontaneously scatter photons is proportional to I_p/Δ^2. This means that $\Gamma/V_0 \propto 1/\Delta$, and hence the ratio of the spontaneous scattering rate to the trap depth can be made small by working at a large detuning.

Apart from the radial trapping force, there is also a longitudinal force acting on the atoms. Owing to the much larger length scale in that direction (given by the Rayleigh length z_R), however, this force is far smaller than the radial one. In order to confine the atoms tightly in all spatial directions, one can use two (or more) crossed dipole traps or superpose an additional magnetic trap. Forced evaporative cooling can be achieved by continuously lowering the trap depth (i.e., decreasing the laser intensity).

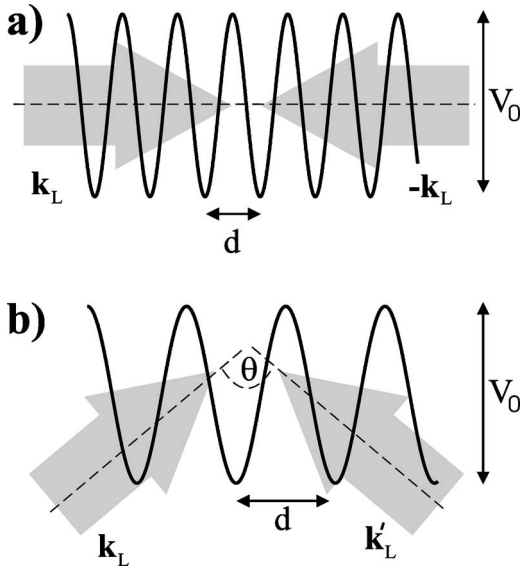

FIG. 1. A one-dimensional optical lattice created from counterpropagating laser beams (a) and with beams enclosing an angle θ (b). The parameters V_0 (lattice depth) and d (lattice spacing) are defined in the text.

2. A simple 1D lattice

Let us now consider what happens when we take two identical laser beams of peak intensity I_p and make them counterpropagate in such a way that their cross sections overlap completely (see Fig. 1). Furthermore, we arrange their polarizations to be parallel. In this case, we expect the two beams to create an interference pattern, with a distance $\lambda_L/2$ between two maxima or minima of the resulting light intensity. The potential seen by the atoms is then simply

$$V(x) = V_0\cos^2(\pi x/d), \tag{5}$$

where the lattice spacing $d=\lambda_L/2$ and V_0 is the lattice depth. Typically, rather than calculating the lattice depth V_0 from the atomic polarizability through Eq. (1), one uses the saturation intensity I_0 of the transition and obtains

$$V_0 = \zeta\hbar\Gamma\frac{I_p}{I_0}\frac{\Gamma}{\Delta}, \tag{6}$$

where the prefactor ζ of order unity depends on the level structure of the atom in question through the Clebsh-Gordan coefficients of the various possible transitions between sublevels.

Let us look at the potential described by Eq. (5) more closely now and define some key parameters. Two obvious quantities associated with this potential are the lat-

[8]For a comprehensive review on dipole traps, see Grimm *et al.* (2000).

tice depth V_0, which measures the depth of the potential from a peak to a trough, and the lattice spacing d. Typically, the lattice depth is measured[9] in units of the recoil energy

$$E_R = \frac{\hbar^2 \pi^2}{2md^2}, \tag{7}$$

and often the dimensionless parameter $s = V_0/E_R$ is used. Making a power series expansion around a potential minimum (e.g., at $x = d/2$) we find, in analogy with our calculation of the dipole trap frequency derived in the previous section, that

$$\omega_{\text{lat}} = \frac{\pi}{d}\sqrt{\frac{2V_0}{m}} \tag{8}$$

gives the harmonic oscillation frequency of an atom trapped inside one of the lattice wells. Comparing this to the frequency $\omega_\perp$ of the dipole trap, we see that both contain the inverse of their respective length scales. From the previous section we know that for a typical dipole trap with $\omega_0 = 10\ \mu$m, frequencies up to a few hundred Hz are possible. The length scale d of a lattice with $\lambda_L = 800$ nm is roughly 20 times smaller. This means that with the same laser intensity, we can realize a trap that (locally) has a harmonic trapping frequency of up to a few kHz.

3. Technical considerations

In practice, a one-dimensional optical lattice can be created in several ways. The easiest option is to take a linearly polarized laser beam and retro-reflect it with a high-quality mirror. In order to be able to control the intensity of the beam and hence the lattice depth, one can use an acousto-optic modulator (AOM). This device allows for a precise and fast (less than a microsecond) control of the lattice beam intensity and introduces a frequency shift of the laser light of tens of MHz.

If the retro-reflected beam is replaced by a second phase-coherent laser beam (which can be obtained, for instance, by dividing a laser beam in two with a polarizing beam splitter and using a wave plate to obtain the correct polarization), another degree of freedom is introduced. It is now possible to have a frequency shift $\Delta\nu_L$ between the two lattice beams. The periodic lattice potential will now no longer be stationary but move at a velocity

$$v_{\text{lat}} = d\Delta\nu_L. \tag{9}$$

If the frequency difference is varied at a rate $d\Delta\nu_L/dt$, the lattice potential will be accelerated with

$$a_{\text{lat}} = d\frac{d\Delta\nu_L}{dt}. \tag{10}$$

Clearly, in the rest frame of the lattice there will be a force $F = ma_{\text{lat}}$ acting on the condensate atoms. We shall see later that this gives us a powerful tool for manipulating a BEC inside an optical lattice.

Another degree of freedom of a 1D lattice realized with two laser beams is the lattice constant. The spacing $d = \lambda_L/2$ between two adjacent wells of a lattice resulting from two counterpropagating beams can be enhanced by making the beams intersect at an angle $\theta < 180°$ [see Fig. 1(b)]. Assuming that the polarizations of the two beams are perpendicular to the plane spanned by them, this will give rise to a periodic potential with lattice constant $d(\theta) = d/\cos(\theta/2)$. To simplify the notation, in this review we shall always denote the lattice constant by d (and all the quantities derived from it, particularly E_R) regardless of the lattice geometry that was used to achieve it.

4. General and higher-dimensional potentials

Up to now we have only considered one-dimensional lattices. Naturally, by adding more laser beams one can easily create two- or three-dimensional lattices. In fact, in the early experiments with near-resonant lattices, a huge variety of different geometries was tested (Jessen and Deutsch, 1996; Meacher, 1998). Experiments with BECs in far-detuned lattices, however, have so far only used a very simple extension to the one-dimensional scheme discussed above. This extension consists in adding a set of laser beams perpendicular to the first pair in order to create a 2D lattice, and yet another pair along the third spatial direction. The interference pattern created by more than three laser beams is rather complicated and depends sensitively on the polarizations and relative phases of the beams and on their orientation. This dependence can be exploited to realize a variety of lattice geometries, but a simpler approach consists in building up the lattice potentials from pairs of independent laser beams. This can be achieved by introducing a frequency offset (using AOMs) of several tens of MHz between the pairs of lattice beams. Interference effects in directions other than the desired lattice directions are then washed out because they move much faster than the typical oscillation frequency of the atoms in the lattice wells.

As an example, Fig. 2 shows two very different two-dimensional potentials created with the same geometry of two sets of counterpropagating lattice beams at right angles to each other. By changing the angle between the polarizations of the two beam pairs, one can create very different potentials. The relative phase between the two standing waves is an additional degree of freedom which can be exploited to control the topology of the potential (Greiner *et al.*, 2001a, 2001b). This, in fact, requires an active (interferometric) stabilization of the phases, since any phase variation will result in a deformation of the potential. A 2D potential can be realized more simply

[9]Note that different conventions and symbols (such as E_{rec}, E_r, and E_0) are found in the literature, often differing by factors of 4 or 8 from the convention used in this review. The reader is advised to check the definition in each paper carefully.

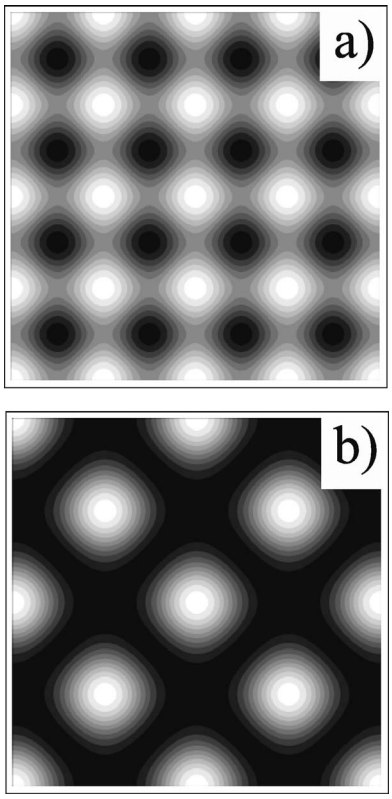

FIG. 2. Examples of two-dimensional potentials created by two alternative methods. In (a), the polarizations of the two waves are orthogonal, i.e., two noninterfering lattices are superimposed. In (b), on the other hand, the polarizations are parallel to each other, leading to four-beam interference. The potential shown in (a) can also be realized with parallel polarizations and a (large enough) frequency difference between the two standing waves.

by introducing a frequency difference between the two beam pairs that is much larger than the trapping frequencies of the wells (see above).

The creation of one-, two-, and three-dimensional periodic structures in which atoms can be trapped and accelerated, with the possibility of switching or modulating the lattice at will, already gives the experimenter great flexibility. But that is not all. By adding a few extra laser beams and/or controlling the polarizations and relative phases of the lattice beams, even more complex potentials, such as quasiperiodic or *kagomé* lattices, can be realized (Santos *et al.*, 2004).

By controlling the polarizations of the lattice beams, it is also possible to create state-dependent potentials that can be shifted relative to each other (Jaksch *et al.*, 1999; Mandel *et al.*, 2003b). In order to obtain such a potential, one uses two linearly polarized laser beams whose polarization vectors enclose an angle θ. This configuration leads to a superposition of σ^+ and σ^- standing waves with associated potentials $V_+(x,\theta)=V_0\cos^2(kx+\theta/2)$ and $V_-(x,\theta)=V_0\cos^2(kx-\theta/2)$ whose relative position depends on θ, which, in an experiment, can be controlled through an electro-optical modulator.

C. Why study BECs in optical lattices?

In the last section of this brief tutorial introduction, we want to make some general comments about the physical concepts associated with condensates in lattices and point out why it is worthwhile studying these systems. The question that forms the title of this section can be asked in two different ways: "Why study condensates in *optical lattices*?" and "Why study *condensates* in optical lattices?" We shall try to answer both of them.

Since optical lattices have been around for longer than BECs, let us start with the latter of the two questions. What is the difference between putting ultracold atoms, on the one hand, or BECs, on the other hand, into optical lattices? First of all, we can say that the temperatures and densities of ultracold atoms and BECs differ considerably. For cold atoms, temperatures are in the micro-Kelvin regime and densities are around 10^{10} cm^{-3}, whereas for BECs typical values are on the order of tens to hundreds of nano-Kelvins for the temperature and up to 10^{14} cm^{-3} or more for the densities. This order-of-magnitude difference in the physical parameters has several consequences. First, lower temperatures mean that a BEC will usually be in the lowest energy levels of the lattice wells without the need for further cooling after the lattice is applied. Second, the higher densities lead to an increased filling factor of the lattice, which can easily exceed unity for BECs, whereas for ultracold atoms filling factors are usually around 10^{-3}. So, rather than ending up with a light-bound "crystal" with lots of vacancies, after applying the lattice each site will be occupied. Third, higher densities also imply that effects due to interatomic interactions can become important. Typical effects associated with the periodicity of the lattice, such as Bloch oscillations and Landau-Zener tunneling (see Sec. VI.D.1), are appreciably influenced by atom-atom interaction. Thus, putting BECs rather than "just" cold atoms into an optical lattice immediately leads to much richer physics as a nonlinearity is introduced into the problem.

Approaching the problem from the other end and starting with Bose-Einstein condensates, we can ask why it is interesting to study them in optical lattices. The immediate answer is that in this way (a) one adds a new length scale to the system, namely, the lattice spacing d, which is typically less than a micron and therefore much smaller than the BEC itself, and (b) periodicity is introduced where before we only had harmonic confinement. The new length scale d leads to very large local trapping frequencies, and in the limit of large lattice depths it is possible to have completely isolated minicondensates that do not interact (or only very weakly) through tunneling. The periodicity, on the other hand, makes it possible to study, for instance, models originally developed in condensed matter physics such as the Bose-Hubbard model, which predicts a quantum phase transition between a superfluid and a Mott insulator.

Many features of condensates in lattices are manifestations of more general concepts of nonlinear systems, such as solitonic propagation and instabilities. Quite a

few of these are also important in nonlinear optics, and we shall point out these similarities throughout this review.

In general, we can say that optical lattices offer several advantages: a vast number of potentials can be created with almost complete control over the parameters (such as lattice depth and spacing), and the potential can be altered or switched off entirely during the experiment. At least the latter feature is certainly not available in *any* solid-state experiment, making optical lattices also an ideal test bed for condensed matter theories.

With these general remarks we end this tutorial introduction, hoping to have prepared the reader for the more systematic and technical account that forms the remainder of this review.

III. THEORY I: GENERAL CONSIDERATIONS

After the general introduction of the first section, we discuss in more detail the theoretical description of a Bose-Einstein condensate in periodic potentials. We mainly concentrate on the physical situation in which we deal with a very large number of atoms. In this case, atom number fluctuations are negligible and a mean-field approach can be used. We only briefly discuss the situation in which quantum fluctuations are crucial (Bose-Hubbard model) at the end of this section.

The general mathematical description of BEC of a weakly interacting gas has already been addressed in different review articles (Dalfovo *et al.*, 1999; Leggett, 2001). In this review we, therefore, concentrate on the results obtained for a BEC in periodic potentials.

The mathematical description of the interacting many-particle system under consideration is significantly simplified due to the fact that the interaction term between the particles results from binary collisions at low energies. These collisions can be characterized by a single parameter, the *s*-wave scattering length (in the following denoted by a_s), which is independent of the details of the two-body potential. This approximation leads to the many-body Hamiltonian describing N interacting bosons in an external trapping potential V_{ext},

$$\hat{H} = \int d^3x \hat{\psi}^\dagger(\mathbf{x}) \left[-\frac{\hbar^2}{2m}\nabla^2 + V_{\text{ext}} \right] \hat{\psi}(\mathbf{x}) + \frac{1}{2}\frac{4\pi a_s \hbar^2}{m} \int d^3x \hat{\psi}^\dagger(\mathbf{x}) \hat{\psi}^\dagger(\mathbf{x}) \hat{\psi}(\mathbf{x}) \hat{\psi}(\mathbf{x}), \tag{11}$$

with $\hat{\psi}(\mathbf{x})$ a boson field operator for atoms in a given internal atomic state. The ground state of the system, as well as its thermodynamic properties, can be calculated from this Hamiltonian. In general these calculations can get very complicated and, in most cases, impracticable. In order to overcome the problem of solving exactly the full many-body Schrödinger equation, mean-field approaches are commonly developed. A detailed derivation can be found in Dalfovo *et al.* (1999).

The basic idea for a mean-field description of a dilute Bose gas was formulated for the homogeneous case $V_{\text{ext}}=0$ by Bogoliubov (1947). The generalization of the original Bogoliubov description to the physical situation in real experiments, i.e., including nonuniform and time-dependent configurations, is given by describing the field operators in the Heisenberg representation by

$$\hat{\Psi}(\mathbf{x},t) = \psi(\mathbf{x},t) + \delta\hat{\Psi}(\mathbf{x},t), \tag{12}$$

where $\psi(\mathbf{x},t)$ is a complex function defined as the expectation value of the field operator, i.e., $\psi(\mathbf{x},t)=\langle\hat{\Psi}(\mathbf{x},t)\rangle$, and its modulus represents the condensate density through $n_0(\mathbf{x},t)=|\psi(\mathbf{x},t)|^2$ [i.e., $N_t=\int|\psi(\mathbf{x},t)|^2 d^3x$, with N_t the total number of atoms]. The function $\psi(\mathbf{x},t)$ is a classical field and is often called the "macroscopic wave function of the condensate." This description is particularly useful if $\delta\hat{\Psi}(\mathbf{x},t)$ is small, meaning that the so-called quantum depletion of the condensate is small. We shall see in the following that for BECs in optical lattices this assumption can become invalid in the context of very deep periodic potentials.

In the limit of negligible depletion of the condensate, the time evolution of the condensate wave function $\psi(\mathbf{x},t)$ (normalized to the total atom number) at temperature $T=0$ is obtained by taking the ansatz for the field operator given in Eq. (12) and using the Heisenberg equation $i\hbar\partial\hat{\psi}(\mathbf{x})/\partial t=[\hat{\psi},\hat{H}]$. This leads to the celebrated Gross-Pitaevskii equation for the mean field $\psi(\mathbf{x},t)$,

$$i\hbar\frac{\partial}{\partial t}\psi(\mathbf{x},t) = \left(-\frac{\hbar^2\nabla^2}{2m} + V_{\text{ext}}(\mathbf{x}) + g|\psi(\mathbf{x},t)|^2 \right)\psi(\mathbf{x},t),$$

$$g = \frac{4\pi\hbar^2 a_s}{m}. \tag{13}$$

In the context of one-dimensional periodic potentials, a further simplification can be obtained by assuming a quasi-one-dimensional situation. This description is valid if the BEC is confined in a cylindrically symmetric trap with a transverse trapping frequency $\omega_\perp$ and negligible longitudinal (axial, x direction) confinement.[10] Additionally, the energy arising from the atom-atom interaction has to be smaller than the energy splitting of the transverse vibrational states $E_\perp=\hbar\omega_\perp$. Within this approximation, the radial part $\psi_\perp(y,z)$ of the macroscopic wave function $\psi=\psi_\perp(y,z)\psi_x(x)$ can be described by a Gaussian having a width corresponding to the transverse ground state. The resulting equation (Steel and Zhang, 1998) is given by

$$i\hbar\frac{\partial}{\partial t}\psi_x(x,t) = \left(-\frac{\hbar^2}{2m}\frac{\partial^2}{\partial x^2} + V_{\text{ext}}(x) \right)\psi_x(x,t) + g_{1\text{D}}|\psi_x(x,t)|^2\psi_x(x,t),$$

[10] In this context, "negligible" means that the periodic potential in the longitudinal direction is only slightly modified by the additional harmonic potential over the extent of the BEC. In practice, this will usually mean that the longitudinal harmonic trapping frequency is of the order of a few Hz.

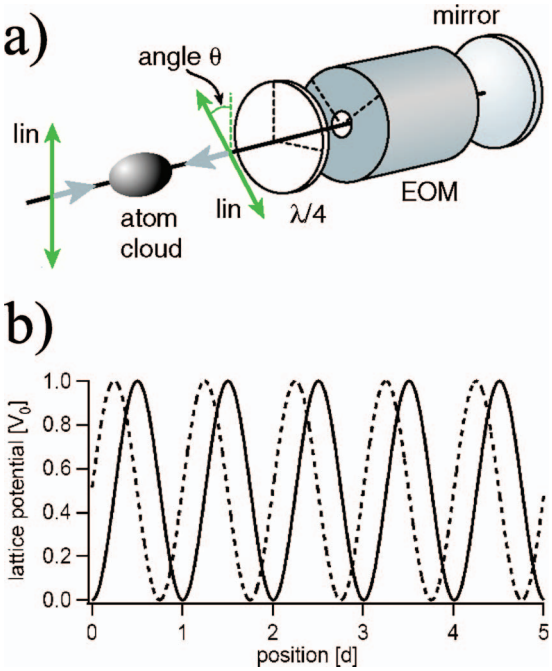

FIG. 3. (Color) Realization of a spin-dependent potential (a) and resulting potential V_+ (b) for $\theta=0°$ (solid line) and $\theta=45°$ (dashed line). Adapted from Mandel *et al.*, 2003b.

$$g_{1D} = 2a_s\hbar\omega_\perp. \tag{14}$$

Thus the condition that the interaction energy must be smaller than the energy splitting of the transverse vibrational states implies that the linear density of the condensate is limited to $n_{1D}<1/2a_s$, which in the case of rubidium ($a_s=5.7$ nm) leads to a maximum linear density of ≈ 100 atoms/μm. In most of the experiments, this simple situation is not realized.

It has been shown that it is also possible to assume the transverse state to be in the self-consistent ground state [nonlinearity is not negligible, see Baym and Pethick (1996)]. This also reduces the description to one dimension, but one ends up with a nonpolynomial nonlinear Schrödinger equation (Salasnich *et al.*, 2002). Nonpolynomial implies that the nonlinear term in Eq. (14) is modified, $|\psi_x|^2 \rightarrow |\psi_x|^2/\sqrt{1+2a_sN_t|\psi_x|^2}$, and an additional nonlinear term appears, given by $\hbar\omega_\perp/2[1/\sqrt{(1+2a_sN_t|\psi_x|^2)}+\sqrt{(1+2a_sN_t|\psi_x|^2)}]$.

Before discussing how the Gross-Pitaevskii equation can be used to describe *nonlinear* phenomena in a BEC, we first give a brief overview of the *linear* theory of a single particle in a periodic potential. Since the nontrivial dynamics of BECs in optical lattices results from the interplay between the discrete translational invariance of the periodic potential (which is a linear property) and the nonlinearity arising from the interatomic interaction, the knowledge of the linear propagation properties is an essential prerequisite for understanding the dynamics of BECs in optical lattices.

IV. THEORY II: THE LINEAR CASE

A. The band structure

The description of the propagation of noninteracting matter waves in periodic potentials is straightforward once one has found the eigenstates and corresponding eigenenergies of the system.

For simplicity we shall restrict our discussion to a one-dimensional *sinusoidal* periodic potential of the form

$$V_{\text{ext}} = V_0\cos^2(kx) = sE_R\cos^2(kx), \tag{15}$$

with $k=\pi/d$, where d is the periodicity of the potential. The extension to two- and three-dimensional situations and even nonsinusoidal potentials is straightforward.

The method for finding the eigenenergies and eigenstates of this system is described on the first pages of almost any textbook on solid-state physics—after all, electrons in a solid also move within a periodic potential (which, in that case, is produced by the crystal ions). In the context of ultracold atoms in standing light waves, this connection was discussed in the early days of atom optics (Letokohov and Minogin, 1977; Wilkens *et al.*, 1991).

The stationary solutions are found in a simple way by applying Bloch's theorem, which states that the eigenwave-functions have the form

$$\phi_{n,q}(x) = e^{iqx}u_{n,q}(x), \tag{16}$$

where q is referred to as quasimomentum[11] and n indicates the band index, the meaning of which will become clear in the following discussion. The functions $u_{n,q}(x)$ are periodic with period d, i.e., $u_{n,q}(x+d)=u_{n,q}(x)$. This allows us to rewrite the wave function and the potential in a Fourier series, with the reciprocal-lattice vector defined by $G=2\pi/d$,

$$\Phi_{n,q}(x) = e^{iqx}\sum_m c_m^n e^{imGx},$$

$$V(x) = \sum_m V_m e^{imGx}. \tag{17}$$

Putting this ansatz for the eigenfunctions into the Schrödinger equation and truncating the sum at $|m|=\mathcal{N}$, one ends up with a $2(2\mathcal{N}+1)$-dimensional system of linear equations,

$$\left\{\frac{\hbar^2}{2m}(q-mG)^2+V_0\right\}c_{q-mG}+V_Gc_{q-(m+1)G} + V_{-G}c_{q-(m-1)G} = Ec_{q-mG}, \tag{18}$$

with $m=-\mathcal{N},-\mathcal{N}+1,\ldots,\mathcal{N}-1,\mathcal{N}$, and for the chosen potential of Eq. (15) one finds $V_{\pm G}=V_0/4$ and $V_{m=0}=V_0/2$. For a given quasimomentum q, this equation leads to

[11]Strictly speaking, $\hbar q$.

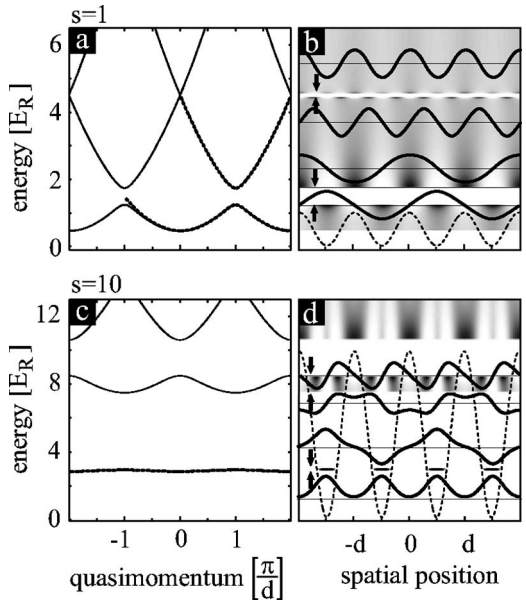

FIG. 4. Band structure for different potential depths: (a) weak potential with $s=1$, (c) deep potential with $s=10$. In both cases, the closed formulas given in the text are depicted with the dotted line. In graphs (b),(d) we visualize the spatial dependence of the corresponding Bloch states. The periodic potentials are represented by the dashed lines. For each energy, the absolute square value of the corresponding Bloch states is depicted in the gray scale plot (high probability is represented by black). Additionally, the wave functions are shown for the energies at the gaps indicated with the arrows. One clearly sees that the wave functions at the first gap change sign from well to well, i.e., there is a phase slip of π. These modes are also known as "staggered modes."

$2\mathcal{N}+1$ different eigenenergies usually referred to as the band energies E_n with $n=0,1,\ldots,2\mathcal{N}$. Each eigenenergy has a corresponding eigenfunction that is given by the Fourier components c^n_{q-mG}.

The eigenenergies and eigenstates depend on the potential depth V_0 and, additionally, on the quasimomentum q. In Fig. 4, we summarize the properties of the eigenbasis for a shallow potential $V_0=E_R$ and a deep potential $V_0=10E_R$. Obviously the presence of a periodic potential significantly modifies the energies of a free particle. The eigenenergies form bands that are separated by a gap in the energy spectrum, i.e., certain energies are not allowed.

In the *weak potential* limit [see Fig. 4(a)], the eigenenergies depend critically on the quasimomentum q. Since the so-called gap energy E^n_{gap} between the nth and $(n+1)$th band scales with V_0^{n+1} in the weak potential limit (Giltner *et al.*, 1995), it only has appreciable magnitude between the lowest and first excited band. Thus a particle with high energy is very well described as a free particle and the influence of the periodic potential is negligible in this case.

In the weak potential limit, the band structure is approximately given by

$$\frac{E(\tilde{q})}{E_R}=\tilde{q}^2 \mp \sqrt{4\tilde{q}^2+\frac{s^2}{16}}, \tag{19}$$

with $\tilde{q}=q/k-1$ and $s=V_0/E_R$. The minus (plus) sign gives the lowest (first excited) band. This well-known result can be found in Ashcroft and Mermin (1976) and is depicted in Fig. 4 with the dotted line. In this graph a constant energy was added to the energy given in Eq. (19) in order to match the numerically obtained band structure.

In Fig. 4(b), we depict the energies in real space. In the same graph we have added information on the real space probability distribution of the eigenfunctions. The gray scale was chosen in such a way that areas with high probability are dark. It is apparent that the eigenfunctions at the lowest and highest energy are almost constant, which implies that the atomic wave function is mainly given by a plane wave corresponding to an "almost" free particle. It is important to note that for energies near the upper band edge of the lowest band, the probability distribution is periodic and its maxima coincide with the potential minima. For this energy we additionally depict the wave function, which reveals that the relative phase of adjacent potential minima is π. This is the well-known sinusoidal Bloch state at the band edge (Brillouin zone edge). In the literature this Bloch state is also referred to as a "staggered mode," i.e., the phase changes by π between adjacent wells. From this graph one can also see that the Bloch state in the first excited band is also sinusoidal but it is in-phase with the periodic potential. Thus the energy of this state is higher due to the bigger overlap with the periodic potential.

In the limit of *deep periodic potentials*, also referred to as the tight-binding limit, the eigenenergies of the low-lying bands are only weakly dependent on the quasimomentum [see Fig. 4(c)]. The quasimomentum dependence of the lowest band energy can also be given analytically (Zwerger, 2003),

$$\frac{E(q)}{E_R}=\sqrt{s}-2J\cos(qd),$$

$$J=\frac{4}{\sqrt{\pi}}(s)^{3/4}e^{-2\sqrt{s}}. \tag{20}$$

This energy expression, in which a constant energy was added, is plotted in Fig. 4(c) as a dotted line and reveals the good agreement with the numerically obtained eigenenergies. The corresponding eigenfunctions are depicted on the right-hand side. Although the absolute value of the eigenfunctions for the lowest band shows no significant dependence on the quasimomentum, the wave functions at $q=0$ and at $q=\pi/d$ differ by the relative phase between adjacent potential minima [see solid lines in Fig. 4(d)]. As in the weak periodic potential limit, the wave function at the upper band edge of the lowest band is staggered, i.e., there is a π phase jump between different sites.

Typical phenomena studied in this regime only involve the lowest band, which is well described by local-

ized wave functions at each site. Therefore, in this limit the dynamics can be described using the localized Wannier functions, which are given as a superposition of the Bloch functions defined in Eq. (16),

$$\phi_n(R,x) = \frac{1}{d}\int dq e^{-iRq}\Phi_{n,q}(x), \tag{21}$$

where R indicates the center of the Wannier function. The dynamics is described via interwell tunneling. The characteristic energy scale of tunneling coupling between two sites is given by the width of the band, which is $4J$.

The linear properties of the periodic potential are uniquely defined by the potential modulation depth V_0. In the following, we distinguish between the weak periodic potential and the deep periodic potential limit. The transition between these two extreme regimes is continuous and thus no well-defined boundary can be given. A characteristic potential modulation for this transition may be found by equating the bandwidth and the gap energy, which have the same magnitude at a potential modulation depth of $V_0 = 1.4E_R$.

B. Dynamics in the linear regime

For the theoretical description of linear matter-wave propagation, we shall distinguish between the situation in which only Bloch states in one band are involved (*intraband* dynamics) and *interband* dynamics, which involves processes leading to a variation of the band populations. Moreover, we shall discuss the dynamics when an additional external potential is present.

1. Intraband dynamics: Pure periodic potential

Generally the description in the linear regime is very simple, because the momentum wave function changes in time solely due to the momentum-dependent energy, which results in a phase factor linearly increasing in time for each momentum. Thus the temporal evolution of a wave packet in an optical lattice can be described by decomposing the initial wave function into Bloch states with the corresponding amplitude $f_n(q)$, and the subsequent evolution is purely a consequence of the accumulated phase $\phi_{n,q}(t) = E_n(q)t/\hbar$,

$$\psi(x,t) = \sum_n \int_{-\pi/d}^{\pi/d} dq f_n(q)\Phi_{n,q}(x)e^{i\phi_{n,q}(t)}. \tag{22}$$

Obviously, if the width of the quasimomentum distribution of the wave function is comparable to the Brillouin zone width, the dynamics cannot be condensed into a simple analytic formula but can still be computed numerically in a straightforward way.

The description becomes very simple if the quasimomentum distribution only involves a small range of quasimomenta centered around q_0 (as indicated in Fig. 5) and only one band (e.g., the lowest band) is involved. In solid-state physics, this is also known as the semiclassical approximation. In this case, the energy dispersion relation (band structure) can be approximated by a Taylor expansion as

$$E(q) = E(q_0) + (q-q_0)\left.\frac{\partial E(q)}{\partial q}\right|_{q_0} + \frac{(q-q_0)^2}{2}\left.\frac{\partial^2 E(q)}{\partial q^2}\right|_{q_0} + \cdots . \tag{23}$$

Furthermore, we assume that $\Phi_{n,q}(x) \approx u_{q_0}(x)e^{iq_0x}$. This approximation neglects the temporal evolution on the length scale of the periodicity. Consequently, the dynamics of the wave packet is given by

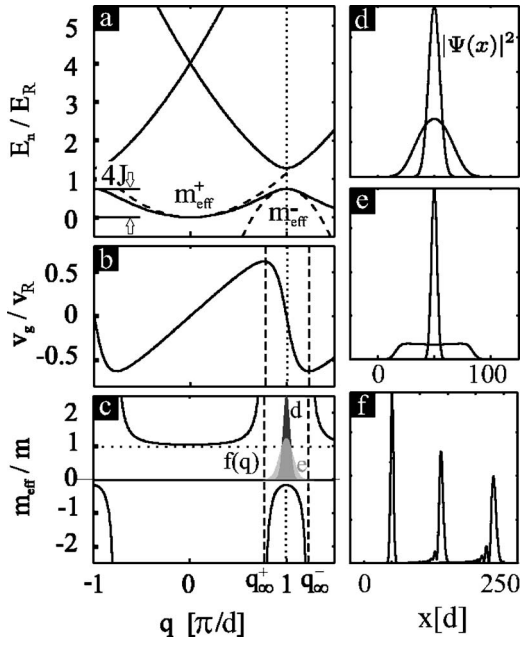

FIG. 5. Summary of the linear propagation of a wave packet in a weak periodic potential. (a) The band structure corresponding to $s=1$, which can be harmonically approximated at $q=0$ and $q=\pi/d$. This corresponds to the effective-mass approximation. (b) The group velocity (in units of $v_R=\hbar k/m$) corresponding to the lowest band reveals that at the center and at the edge of the Brillouin zone the wave packet does not move. Additionally, the velocity in the lowest band is limited to a maximum velocity. (c) The spreading of a wave packet is a consequence of the group velocity dispersion described by the effective mass. The effective mass can be *larger* (and, indeed, even infinite at $q^{\pm}_{\infty}$) than the free mass, but also *smaller* and negative at $q=\pi/d$. The evolution of the wave packets for the momentum distributions indicated in black (gray) shading is shown in (d) [(e)]. (d) The real space evolution of the envelope of the wave packet prepared in the region of constant effective mass. The wave packet spreads without distortion. (e) If the broad quasimomentum distribution does not allow the quadratic approximation of the energy, higher-order terms in the Taylor expansion become relevant and lead to a distortion of the wave packet. (f) The evolution of a wave packet prepared at the infinite mass point $q_0=q^+_\infty$ for a propagation time 2.5 and 5 times longer than that of (d) and (e). This wave packet moves with the maximum velocity associated with the lowest band and reveals strongly suppressed spreading.

TABLE I. Analytical solutions for the effective masses at the center ($q=0$) and the Brillouin zone edge ($q=\pi/d$).

$s[V_0/E_R]$	$m_{\mathrm{eff}}/m(q=0)$	$m_{\mathrm{eff}}/m(q=\pi/d)$
0–3	$\dfrac{1}{1-\dfrac{2}{\sqrt{4+s^2/16}}+\dfrac{8}{(4+s^2/16)^{3/2}}}$	$\dfrac{1}{1-\dfrac{8}{s}}$
5–∞	$\dfrac{\hbar^2}{2d^2J}$	$-\dfrac{\hbar^2}{2d^2J}$

$$\psi(x,t)=u_{q_0}(x)e^{-(i/\hbar)E(q_0)t}\times\int dqf(q)e^{-i(q-q_0)[x-v_g(q_0)t]-i[\hbar(q-q_0)^2/2m_{\mathrm{eff}}(q_0)]t}, \tag{24}$$

where we have defined

$$v_g(q_0)=\frac{1}{\hbar}\left.\frac{\partial E(q)}{\partial q}\right|_{q_0} \tag{25}$$

and

$$m_{\mathrm{eff}}(q_0)=\hbar^2\left(\left.\frac{\partial^2E(q)}{\partial q^2}\right|_{q_0}\right)^{-1}. \tag{26}$$

From Eq. (24), we conclude that the wave packet moves with the group velocity v_g. In analogy to the spreading of a wave packet in free space due to the dispersion relation $E=\hbar^2k^2/2m$, the matter wavelet in the optical lattice also spreads, but with a modified dispersion described by the effective mass. In Fig. 5, the group velocity and effective mass are also depicted.

For the special cases corresponding to the central quasimomenta $q_0=0$ and $q_0=\pi/d$, the wave packet does not move and spreads as in free space, albeit with a modified mass. It is important to note the effective mass at $q=0$ is positive and *larger* than the free mass, while at $q=\pi/d$ it is negative and its absolute value is smaller than the free-particle mass (for weak potentials, $V_0<4E_R$). For a given potential depth, there exists a quasimomentum q_∞ where the group velocity is extremal, which implies that the second derivative of the dispersion relation is zero and thus the effective mass diverges. In other words, linear wave packets prepared at $q=q_\infty$ move with the maximum velocity allowed in the lowest band and do not spread in first approximation. Generally higher-order terms in the Taylor expansion Eq. (23) need to be taken into account, which eventually leads to a distortion of the wave packet on a longer time scale [see Fig. 5(f)].

For both shallow and deep periodic potentials, closed formulas for the effective masses can be derived and are given in Table I.

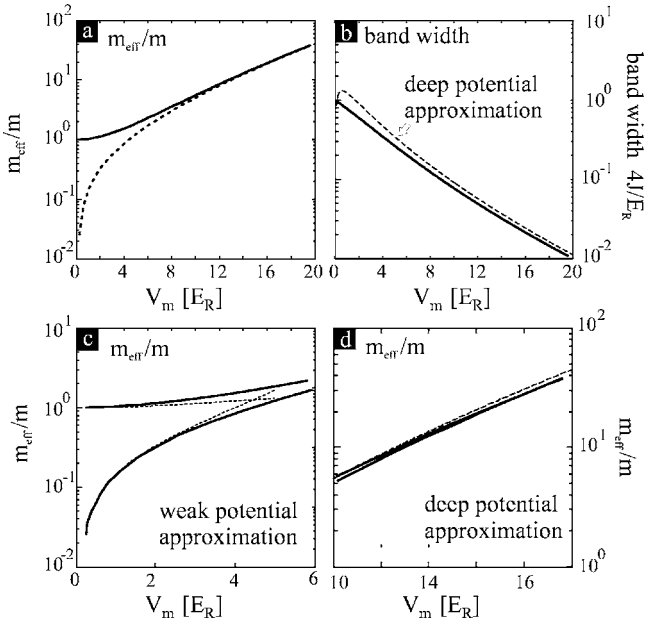

FIG. 6. Characteristic linear energies as a function of potential modulation depth. (a) Numerically calculated absolute value of the effective mass for the center $q=0$ (solid line) and the edge $q=\pi/d$ (dashed line) of the Brillouin zone where the mass is negative. The analytical results discussed in the text are represented by the dashed lines in (c) and (d). For potentials with deep modulation, the absolute values of the masses become equal and there is no quasimomentum dependence. (b) The width of the band decreases exponentially with increasing potential modulation depth. In the deep potential limit, this energy scale is associated with the tunneling rate between two adjacent wells.

In the context of deep optical lattices, the description can be significantly simplified if one treats the dynamics locally, in which case the dynamics is described by tunneling from one well to the next. The tunneling rate J is sometimes also referred to as "hopping rate" and can be calculated by evaluating

$$J\simeq-\int d\mathbf{r}\left[\frac{\hbar^2}{2m}\vec{\nabla}\phi_n\cdot\vec{\nabla}\phi_{n+1}+\phi_nV_{\mathrm{ext}}\phi_{n+1}\right], \tag{27}$$

where ϕ_n are the localized wave functions of the nth potential minimum (normalized to unity). These wave functions are also known as Wannier states [as defined in Eq. (21)] and are *not* Gaussians. In fact, by making a Gaussian ansatz for the local wave function, one overestimates the tunneling rate significantly. In the deep periodic potential limit, there is also a direct connection between the width of the band and the tunneling rate, namely, $E_w=4J$. The comparison of the exact solution for the width of the band representing the characteristic energy for tunneling and the effective mass describing the dispersion of a wave packet are depicted in Fig. 6.

2. Intraband dynamics: With additional potential

The wave-packet dynamics in a periodic potential in the presence of an additional external potential, i.e.,

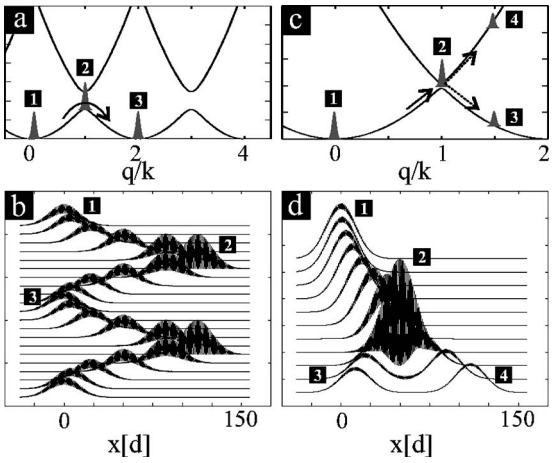

FIG. 7. Wave-packet dynamics in a periodic potential in the presence of a constant force. (a),(b) An external force leads to a variation of the central quasimomentum $q=0$. Since the group velocity changes sign when the quasimomentum exceeds the Brillouin zone, the wave packet will show an oscillatory behavior in real space. This is known as Bloch oscillations and is one example of intraband dynamics. (c),(d) For strong external forces, nonadiabatic transitions to the first excited band can occur near the band edge. This is known as Landau-Zener tunneling and leads to a splitting of the wave packet. All graphs reveal clearly the Bloch state structure. Near $q=0$, the wave packet is only weakly modulated with the period of the periodic potential, while at the band edge it is fully modulated revealing the sinusoidal Bloch state at the Brillouin zone edge.

with an external force, is generally not easy to solve. The problem becomes relatively simple, though, as soon as the width of the wave packet in quasimomentum space is small and thus the wave packet can be characterized by a single mean quasimomentum q_0. The external force then leads to a time-dependent $q_0(t)$ via $\hbar q_0(t)=F_x$. In the case of a constant force F (e.g., due to the gravitational field), this results in $q_0(t)=q_0(t=0)+Ft/m$ (Ashcroft and Mermin, 1976; Scott *et al.*, 2002; Anker *et al.*, 2004). Since the group velocity of a wave packet depends on the quasimomentum, the position of the wave packet continuously changes, as is indicated in Fig. 7. As the group velocity of the wave packet alters sign when the central quasimomentum crosses the Brillouin zone boundary, the result of the force is not an acceleration of the wave packet but leads to oscillations. The latter are known as Bloch oscillations in real space.

Bloch oscillations have also been studied in the regime of deep periodic potential by analyzing a variational Gaussian profile wave packet whose extension is much bigger than the lattice spacing. The equation of motion for the four variational parameters—center-of-mass position, width of the packet, linear phase gradient across the packet, and quadratic phase across the packet—leads essentially to the same result as in the weak potential limit. The motion of a wave packet in an additional harmonic potential has been discussed in the weak potential limit (Anker *et al.*, 2004) and in the deep potential limit (Cataliotti *et al.*, 2001; Trombettoni and Smerzi, 2001; Krämer *et al.*, 2002).

3. Interband dynamics

In the case of a strong external force acting on matter waves in periodic potentials, transitions into higher bands can occur (see Fig. 7). In the context of electrons in solids, this is known as the Landau-Zener breakdown, occurring if the applied electric field is strong enough for the acceleration of the electrons to overcome the gap energy separating the valence and conduction bands.

It was shown by Zener (1932)[12] that for a given acceleration a_{exp} corresponding to a constant force, one can deduce a tunneling probability

$$r=\exp\left(-\frac{a_c}{a_{\mathrm{exp}}}\right), \quad a_c=\frac{V_0^2 d}{16\hbar^2} \tag{28}$$

across the gap[13] in the adiabatic limit. The resulting wave-packet dynamics is shown in Fig. 7, where Landau-Zener tunneling leads to a splitting of the wave function. It has also been shown theoretically and experimentally that the influence of nonlinearity can drastically change this behavior (Wu and Niu, 2000; Morsch *et al.*, 2001; Liu *et al.*, 2002).

V. THEORY III: PERIODIC POTENTIALS AND NONLINEAR THEORY

So far we have only considered the linear regime for which the theoretical description is straightforward and fully defined by the band structure. As we have seen, the equation of motion of the condensate wave function is defined via a nonlinear Schrödinger equation due to the interaction between the particles. This introduces a new energy scale and thus, in contrast to the linear propagation, new parameter regimes with associated new phenomena and dynamics for special potential parameters are expected. One of the most striking of these is the appearance of solitonic propagation (nonspreading wave packets) and instabilities (i.e., small perturbations of the condensate wave function can grow exponentially in time). The "catastrophe" associated with these instabilities implies that the description using a mean-field approach, which assumes that only one wave function is macroscopically populated, becomes invalid. Some examples for this can be found in the review by Brazhnyi and Konotop (2004).

A. Characteristic nonlinear energy

The mean-field energy [see Eq. (11)] per atom corresponding to a given condensate wave function, which is normalized to 1, is defined as

[12]A more recent study can be found in Iliescu *et al.* (1992).

[13]This has been observed experimentally with cold atoms (Niu *et al.*, 1996).

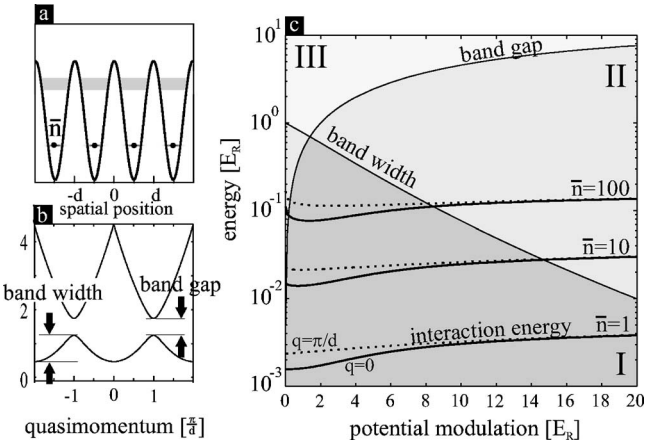

FIG. 8. Characteristic energies as a function of potential modulation depth. (a) $\bar{n}$ represents the number of atoms per site. (b) Definition of bandwidth and band gap. (c) The graph reveals that the linear energy scales—bandwidth and band gap—divide the parameter space into three distinct regimes (dark shading, energy is smaller than band gap and bandwidth; light shading, energy is between band gap and bandwidth; no shading, energy is higher than both characteristic linear energy scales). The on-site interaction energy for different atom numbers per site is also given (assuming a radial trapping frequency of $\omega_\perp = 2\pi \times 200$ Hz). The solid (dotted) line indicates the on-site interaction energy associated with the Bloch state at the Brillouin zone center (edge). With 100 atoms per site, the regimes I and II exhibiting very different dynamics can be explored by simply changing the potential modulation depth.

$$U = g \int d^3x |\psi(\mathbf{x})|^4. \tag{29}$$

In the case of periodic potentials, it is more sensible to calculate the on-site interaction energy, which measures the strength of the interaction within one period of the lattice. The integral in Eq. (29) is then evaluated over one period of the lattice.

In order to obtain an estimate for the on-site interaction energy given in Eq. (29), we assume the following simple situation: The condensate has been realized in a cylindrically symmetric trap with radial trapping frequency $\omega_\perp$ and vanishing longitudinal (along the lattice direction) confinement. The periodic potential is realized in the x direction. Furthermore, we assume that the wave function in the radial direction is described by the self-consistent ground state of the harmonic trap approximated by a Gaussian function as described in Baym and Pethick (1996). In the longitudinal direction, we assume that the wave function does not significantly deviate from the linear Bloch or Wannier states, calculated as discussed in Sec. IV.A. Obviously this is an approximation, but it allows one to estimate at which point the nonlinearity becomes important by comparing this energy to the other characteristic energies of the problem, such as the width of the energy band and the gap energy.

In Fig. 8, we compare the tunneling splitting (energy bandwidth) and the gap energy with the on-site interaction energy as a function of the lattice depth. The dependence of the linear energies can be understood straightforwardly. The gap energy in the limit of deep potentials has to converge to the energy difference between the ground and first excited states near the harmonic minimum of the periodic potential. This is given by $\bar{\omega} = 2\sqrt{s}E_R$. The width of the band is a consequence of the possibility to tunnel from one well to the other. In the limit of deep potentials, this probability will be exponentially small and the bandwidth, therefore, decreases exponentially as a function of potential modulation depth.

In order to get more insight into the absolute energy scales, we now calculate the on-site interaction energy for a typical experimental situation. We assumed a condensate of ^{87}Rb atoms confined in a trap with a transverse trapping frequency of $\omega_\perp = 2\pi \times 200$ Hz. Increasing the atom number per well $\bar{n}$ leads to an increase of the density and thus the on-site energy. The gain in on-site interaction energy does *not* depend linearly on the atom number because the width of the self-consistent ground state will increase as the number of atoms in this state grows, leading to a smaller increase in density. In order to reveal the dependence of this characteristic nonlinear energy on the quasimomentum, we depict in Fig. 8 the two extreme cases $q=0$ and $q=\pi/d$. Obviously, in the deep potential limit no difference is visible, which is expected since the absolute value of the eigen-wavefunctions in the lowest band depends only weakly on the quasimomentum (see Fig. 4). In the limit of weak periodic potentials, the nonlinear energy is higher at the Brillouin zone edge. This is due to the fact that the Bloch states at $q=0$ are hardly modulated, while at the edge of the Brillouin zone the Bloch state is fully modulated (see Fig. 4), leading to an increased local density.

Having introduced the characteristic energies of our problem, we are now in a position to classify BECs in optical lattices using the following three parameters:

(i) Bandwidth $4J$: describes the energy associated with tunneling between adjacent potential minima.

(ii) U: gives the on-site interaction energy per atom on a single lattice site.

(iii) E_{gap}: represents the energy difference between the bands at $q=\pi/d$; in a deep optical lattice this is the energy difference between the lowest and first vibrational state in a single potential well of the lattice.

Although the concept of linear band theory breaks down as soon as the nonlinear energy is no longer the smallest energy scale in the problem, it still allows us to distinguish between different regimes indicated in Fig. 8.

The regime in which the nonlinearity is the *smallest* energy scale is indicated in Fig. 8 by the dark shaded area. Clearly, in practice it is easy to realize experiments in which the nonlinearity is the smallest energy scale. It is more challenging, on the other hand, to enter the regime for which the nonlinearity is *larger* than the band-

width but still *smaller* than the band-gap energy. This can be achieved by increasing the atom number per well or by increasing the transverse trapping frequency. Finally, the third regime—for which the nonlinearity is the largest energy scale—is very difficult to reach with the chosen transverse trapping frequency of $\omega_\perp = 2\pi \times 200$ Hz, since putting more atoms into each well does not significantly increase the density. This is because of the expansion of the self-consistent ground state in the transverse direction with increasing atom number. This regime can, therefore, only be reached by realizing a *high* transverse trapping frequency and a *small* potential modulation depth.

With this classification scheme in mind, we now discuss the theoretical descriptions already existing for these regimes. We start our discussion in the regime that is closest to the linear situation, i.e., for which the nonlinear interaction energy is the smallest energy scale of the problem.

B. Nonlinear energy scale is the smallest

In contrast to what one might naively expect, namely, only a small change of the dynamics due to the presence of the interaction between the atoms, the following will clearly show that nonlinear physics contains a lot of counterintuitive and dramatic phenomena. Since the mathematical description is different for the weak and deep potential limits (similarly to the linear case, see Sec. IV), we will discuss these two regimes separately.

1. Weak periodic potential limit

If the nonlinearity is the smallest energy scale of the system, a simplified description can be found by starting from the linear description of matter wave packets in a periodic potential. As already discussed above, wave packets with a small momentum distribution centered around q_0 in one specific band (for simplicity we assume that $n=0$) are well described by a slowly varying amplitude $A(x,t)$ (on the scale of the periodicity) multiplied by the Bloch state corresponding to the central quasimomentum,

$$\psi(x,t) = A(x,t)\Phi_{n=0,q_0}(x)e^{-(i/\hbar)E(q_0)t}. \tag{30}$$

Assuming this functional dependence, it has been shown in different works (Lenz *et al.*, 1994; Steel and Zhang, 1998; Konotop and Salerno, 2002; Pu *et al.*, 2003) that in the case of weakly interacting matter waves, a nonlinear Schrödinger equation for the envelope $A(x,t)$ can be derived employing "multiple scales analysis" [a general introduction into this theoretical method can be found in Bender and Orszag (1978)]. The resulting differential equation for the envelope has the same form as the Gross-Pitaevskii equation but with a modified linear (dispersion) and interaction energy,

$$i\hbar\left(\frac{\partial A(x,t)}{\partial t} + v_g\frac{\partial A}{\partial x}\right) = -\frac{\hbar^2}{2m_{\text{eff}}}\frac{\partial^2}{\partial x^2}A(x,t) + V(x,t)A(x,t) + g_{1\text{D}}\alpha_{\text{nl}}|A(x,t)|^2A(x,t), \tag{31}$$

where m_{eff} is the effective mass as discussed in Sec. IV.A. The coefficient $\alpha_{\text{nl}} = (1/d)\int_{-d/2}^{d/2}dx|u_{q_0}|^4 \sim 1-2$ describes the renormalization of the interaction energy which increases due to the stronger localization in the periodic potential (see the Bloch states in Fig. 4). This has already been discussed in the context of characteristic nonlinear energy in Sec. V.A, where the dependence of the eigenstates on the quasimomentum led to different characteristic energies (see Fig. 8).

Even though the *stationary* solutions of this equation do not differ significantly from the linear case, the *dynamics* of this system is totally different. Especially noteworthy is the formation of bright solitons, i.e., nonspreading wave packets, even for a repulsive atom-atom interaction provided that the central quasimomentum is in the regime of negative effective mass. In the work by Steel and Zhang (1998), these so-called "gap solitons" in periodic potentials were first predicted. The stability of these gap solitons realized in a quasi-one-dimensional waveguide is analyzed by Hilligsoe *et al.* (2002) and Scott *et al.* (2003). Their main result is that the soliton is destroyed due to coupling to the bands corresponding to the higher transverse vibrational states and by the formation of vortex-antivortex pairs. In this context, we point out that the prediction of solitonic propagation in the regime of anomalous dispersion (i.e., for negative effective mass) was also suggested by Zobay *et al.* (1999). In that work, the use of the velocity dependence of the energy of a gray state resulting from the coupling between two magnetic substates with light was put forward as a way of generating the necessary anomalous dispersion. The appearance of a new class of solitons—also called "out-of-gap solitons"—was predicted by Yulin and Skryabin (2003), who applied the coupled mode description developed in the field of nonlinear optics to the case of Bose-Einstein condensates in periodic potentials.

Another very intriguing phenomenon arising in the presence of nonlinearity is modulational instability. Since this is a very well investigated effect, we shall devote a separate section, Sec. V.E, to this topic. Generally, instability means that a small perturbation on the condensate wave function grows exponentially fast. This can be qualitatively understood on the basis of the given effective nonlinear Schrödinger equation (31) by realizing that this equation implies that a *repulsive* interaction in the negative effective-mass regime leads to an effective *attractive* interaction between the particles with a reversed time evolution. For an attractive interaction it is well known that collapse dynamics can occur, i.e., a small perturbation can grow exponentially fast.

In the work by Konotop and Salerno (2002), this modulational instability is discussed in the context of "multiple scales analysis" and in analogy to nonlinear photon optics. Essentially, it turns out that the instabili-

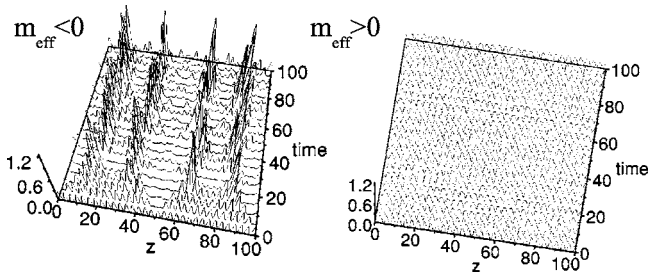

FIG. 9. The temporal evolution of a condensate wave function of repelling atoms prepared in the negative and positive effective-mass regime [from Konotop and Salerno (2002)]. The modulation of the condensate wave function reveals the sinusoidal spatial dependence of the Bloch state at the Brillouin zone edge. Clearly, the initial wave function in the negative mass regime is not stable and decays into bright solitons and background. It is important to note that although the atom-atom interaction is repulsive, nonspreading wave packets are formed. In the positive mass regime (i.e., in the second band at the Brillouin zone edge), the wave function is also spatially modulated, yet no instability is present.

ties can be exploited in order to prepare solitons. In Fig. 9, the temporal evolution of a homogeneous condensate prepared at the edge of the Brillouin zone ($q_0=\pi/d$) is shown. Clearly, the condensate wave function is periodically modulated, revealing the sinusoidal Bloch state at the Brillouin zone edge. Very quickly the wave function breaks up into four localized structures, which represent the gap solitons mentioned above. In Konotop and Salerno (2002), it was also shown that in the positive mass regime the macroscopic wave function is stable against small spatial modulations. It is important to note that a more thorough analysis by Wu and Niu (2001) revealed that in the weak potential limit, effective negative mass (deduced from the linear analysis of the problem) is only a sufficient criterion for modulation instabilities but not a necessary one, i.e., even in the positive mass regime instabilities may arise. This demonstrates the limited range of applicability of the effective-mass approximation for quantitative predictions.

2. Deep periodic potential limit—tight-binding limit

The regime in which the width of the band becomes smaller than the gap energy is usually referred to as the "tight-binding regime." As one can see in Fig. 4, the linear Bloch waves exhibit strong localization in the deep potential limit. This suggests that the ongoing physics becomes more transparent by describing the condensate wave function with localized Wannier states $\Phi_n(\mathbf{x};t)=\phi_{n=1}(R=nd,x)$ [ϕ_n defined in Eq. (21)] associated with the lowest band (Chiofalo *et al.*, 2000; Alfimov *et al.*, 2002a). It is important to note that the strong localization leads to high atomic densities and thus the linear Wannier states are modified due to the presence of the atom-atom interaction. The self-consistent ground state, therefore, depends on the atom number within one potential minimum, and the condensate wave function is better described by

$$\psi(r,t)=\sum_n \psi_n(t)\Phi_n(\mathbf{r};N_n(t)), \tag{32}$$

where the functions $\Phi_n(\mathbf{x};N_n)$ are localized at the nth minimum of the potential and represent the self-consistent ground states within one potential well. By applying this ansatz to the Gross-Pitaevskii equation, Smerzi and Trombettoni (2003) derived a discrete nonlinear equation describing the dynamics through the single amplitudes $\psi_n(t)$. This approach also allows one to describe situations that are not in the true one-dimensional limit [see Eq. (14)] by taking into account the atom number dependence of the transverse width of the wave function.

Since the general differential equation taking into account transverse degrees of freedom is very complicated (Smerzi and Trombettoni, 2003), in the following we shall only discuss the regime in which the local wave function does not depend on the local atom number, corresponding to the zero-dimensional case of Smerzi and Trombettoni (2003), and thus $\Phi_n(\mathbf{r};N_n(t))=\phi_n(\mathbf{r})$. This was already discussed earlier by Trombettoni and Smerzi (2001). The resulting equation is the well-known discrete nonlinear Schrödinger equation

$$i\hbar\frac{d}{dt}\psi_n=J(\psi_{n+1}+\psi_{n-1})+\tilde{U}|\psi_n|^2\psi_n+\epsilon_n\psi_n, \tag{33}$$

which describes the special dynamics arising from the interplay between discreteness and nonlinearity. The basic processes result from next-neighbor coupling due to tunneling described by the parameter J (which is equivalent to the tunneling parameter K used in the cited literature), the on-site linear energy ϵ_n, and the nonlinear coefficient $\tilde{U}=U/N_t$ [note that $\tilde{U}$ is proportional to the characteristic nonlinear on-site energy U given in Eq. (29)],

$$J\simeq-\int d\mathbf{r}\left[\frac{\hbar^2}{2m}(\vec{\nabla}\phi_n\cdot\vec{\nabla}\phi_{n+1})+\phi_n V_{\mathrm{ext}}\phi_{n+1}\right], \tag{34}$$

$$\epsilon_n=\int d\mathbf{r}\left[\frac{\hbar_2}{2m}(\vec{\nabla}\phi_n)^2+V_{\mathrm{ext}}\phi_n^2\right], \tag{35}$$

$$\tilde{U}=gN_t\int d\mathbf{r}\,\phi_n^4, \tag{36}$$

with $g=4\pi\hbar^2a/m$ and N_t the total number of atoms in the condensate.

3. Intraband dynamics: Pure periodic potential

Further insight into the global dynamics of a Bose-Einstein condensate in deep periodic potentials can be gained by studying the temporal evolution of a Gaussian profile which varies slowly on the scale of the periodicity of the potential. This approach is called the collective variable approach (Trombettoni and Smerzi, 2001; Menotti *et al.*, 2003b). The Gaussian wave packet is parametrized by four quantities: the center-of-mass position, the width of the wave packet described by γ (half

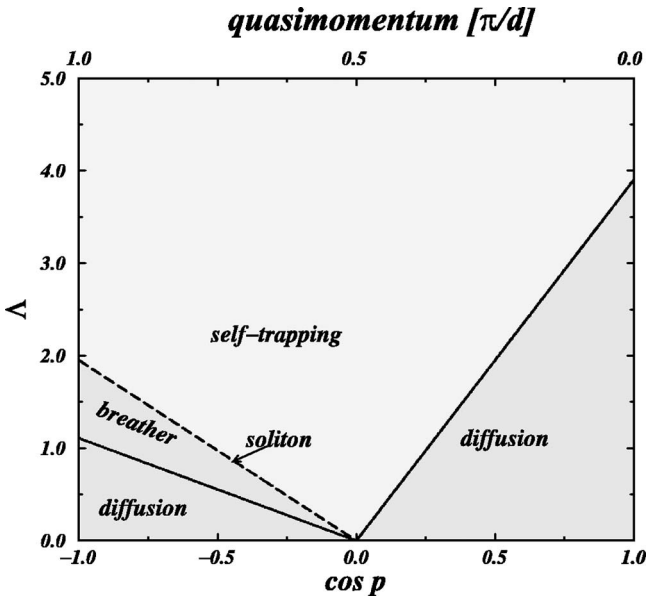

FIG. 10. Classification of the nonlinear propagation in deep periodic potentials [from Trombettoni and Smerzi (2001)]. The propagation of a Gaussian wave packet initially centered around $q_0=p/d$ in a given periodic potential depends critically on the total atom number $\Lambda \propto N_t$ and the quasimomentum q_0. For large nonlinearity, after some initial dynamics the wave packet stops expanding independently of the initial quasimomentum (self-trapping regime). For small nonlinearities (small atom number), the wave packet will expand indefinitely. This is also called the diffusive regime. The solitonic propagation or "breathers" (time periodic and spatially localized excitations) are only possible for quasimomenta with corresponding negative mass. Since this excitation relies on a delicate balance between nonlinearity and linear spreading, it only appears for very well-defined atom numbers.

of the $1/e$ width of the Gaussian wave function), the linear phase describing the group velocity of the wave packet, and the quadratic phase over the wave packet. The latter phase allows us, on the one hand, to describe the linear evolution of the wave packet for which the quadratic dispersion in momentum space directly translates into a quadratic phase in real space. On the other hand, the nonlinear energy due to interaction also leads to a quadratic phase in first approximation since the density near the Gaussian maximum is quadratic.

From the equations of motion for these variational parameters, one can characterize the dynamics by two basic parameters $\cos p$ and Λ. The parameter $\cos p \in [-1,1]$ is directly connected to the quasimomentum $p=qd$ as indicated in Fig. 10. The other parameter is given by $\Lambda=(N_t g/2J)\int d\mathbf{r}\phi_n^4=\tilde{U}/2J$ and arises from the nonlinearity due to the atom-atom interaction. The diagram in Fig. 10 shows the propagation characteristics depending on the two basic parameters and reveals that the resulting evolution can be characterized by diffusion, solitonic propagation, and self-trapping.

The *solitonic evolution* is found by imposing the condition that neither the width nor the quadratic phase is time dependent, which leads to the condition $\Lambda_{\mathrm{sol}}=2\sqrt{\pi}|\cos p|e^{-1/2\gamma_0}/\gamma_0$, where γ_0 represents the $1/e$ width of the initial Gaussian wave function in units of the lattice constant. From this condition equation it follows that the atom number in a soliton is inversely proportional to the width of the soliton. It is important to note that these solitons are very closely related to the solitons discussed in the weak potential limit (Steel and Zhang, 1998; Zobay *et al.*, 1999; Alfimov *et al.*, 2002b).

The *discrete* solitons described here, which populate only a few lattice sites, exhibit a reduced mobility in comparison to the gap solitons described in the weak potential. This is due to the so-called Peierls-Nabarro barrier, which will be discussed below (see Sec. V.C). The qualitative differences between discrete solitons and continuous solitons were pointed out by Dauxois and Peyrard (1993): "The world of discrete solitons is as merciless for the weak as the real world; in the presence of discreteness, breather interactions show a systematic tendency to favor the growth of the large excitation at the expense of the others."

An extension of this treatment to discrete solitons living on a constant background was published by Abdullaev *et al.* (2001). In this work, the authors show that in the limit of deep periodic potentials a small excitation on top of a homogeneous background can also exhibit solitonic propagation. While the solitons discussed above are solutions of the nonlinear Schrödinger equation, the solitons living on the background are solutions of the Korteweg–de Vries equation. This equation is very famous for solitonic propagation since it describes the solitonic waves in water (Russel, 1845).

In the limit we have discussed here, excitations on a condensate have also been studied. The results can be found in Javanainen (1999), Martikainen and Stoof (2003a), and Menotti *et al.* (2003a).

4. Intraband dynamics: With additional potential

The dynamics of a wave packet in a deep periodic potential with an additional harmonic potential in the limit of small oscillations was studied theoretically by Krämer *et al.* (2002). Furthermore, the breakdown of those oscillations for large oscillation amplitudes was investigated by Chiofalo and Tosi (2000, 2001), Smerzi *et al.* (2002), and Menotti *et al.* (2003b).

In the case of small oscillation amplitudes (Krämer *et al.*, 2002), the motion of the condensate wave function is found by employing the tight-binding ansatz [see Eq. (32)] which, for further calculations, is smoothed over the periodicity leading to equations for the envelope of the wave function characterized by the parameters $n_m(x,y,z)$ as the "macroscopic" (smoothed) density, and the "smoothed" phase $S(x,y,z)$ of the wave function.[14]

One very intriguing result is obtained by assuming a constant phase gradient across the condensate wave function and hence a constant phase difference between

[14]Note that in the original publications the periodic potential is applied in the z direction.

adjacent wells, $\partial_x S = P_x(t)/\hbar$ with P_x as a time-dependent parameter. With this assumption, the motion of the center of mass $X(t) = \int dV x n_m(t)/N_t$ is given by

$$\hbar \dot{X} = 2Jd \sin\left(d\frac{P_x}{\hbar}\right),$$
$$\dot{P}_x = -m\omega_x^2 X. \tag{37}$$

This simple differential equation system is well known in the context of the dynamics of superconducting Josephson junctions as the "resistively shunted junction" model (Barone, 2000). In the context of BECs in optical lattices, this was investigated theoretically as well as experimentally by Cataliotti *et al.* (2001). It is important to note that the resulting equation does not depend on the interaction between the atoms and thus describes the linear dynamics of a wave packet oscillating with the corresponding effective mass. The effective-mass approximation is generally applicable for any small-amplitude oscillations [collective excitations (Stringari, 1996)] by replacing $\omega_x \to \omega_x\sqrt{m/m_{\text{eff}}}$, where x indicates that the frequency is only modified in the direction of the periodic potential (Krämer *et al.*, 2002). In order to make an absolute comparison between theory and experiment, care has to be taken when calculating the effective mass or, alternatively, the tunneling parameter J.

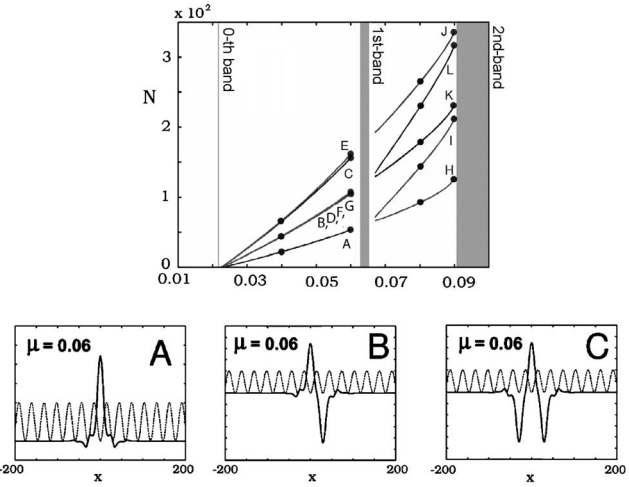

FIG. 11. Selection of stationary solutions in the regime of intermediate nonlinear on-site interaction energy (Louis *et al.*, 2003). Clearly, the atom-atom interaction leads to new stationary solutions whose energies lie in the energy gap of the linear system. Since these are nonlinear solutions, their energies μ depend on the atom number N. The main graph shows that there are different branches of solutions. In the lower three graphs, we show three solutions corresponding to the indicated energies. In contrast to the solutions expected from a tight-binding approximation treatment, they show structure within the potential minima.

C. Nonlinear energy scale in the intermediate range

The regime of self-trapping as indicated in Fig. 10 is defined by the condition that the width of a packet for infinitely long times is finite and does not change in time. This leads to a critical value of the parameter Λ given by $\Lambda_c = 2\sqrt{\pi}\gamma_0 \cos p_0 \exp(-1/2\gamma_0^2)$. The condition $\Lambda < \Lambda_c$ implies that the nonlinear on-site interaction energy per particle is smaller than the width of the band and thus the evolution can be qualitatively described by assuming a wave packet with a mean quasimomentum. We have already mentioned that in this limit the wave packet will just spread (this is the diffusive regime in Fig. 10). In the case of $\Lambda > \Lambda_c$, the on-site interaction energy is larger than the width of the band and thus the description based on a single central quasimomentum fails. Although in these circumstances even the variational approach is a very crude approximation, it still gives a good estimate for the parameters for which this effect will occur. The detailed dynamics in the self-trapping regime is very complicated and involves modulational instabilities [general treatment by Dauxois *et al.* (1997)], the formation of breathers (time periodic and spatially localized excitations), solitons, and so forth (Tsukada, 2002; Menotti *et al.*, 2003b). In spite of the complicated dynamics, the suppression of wave-packet spreading can be attributed to local dynamics at the edges of the wave packets. There macroscopic self-trapping known from Josephson-junction physics (Smerzi *et al.*, 1997) occurs, which effectively leads to "walls" keeping the wave packet together (Anker *et al.*, 2005).

The treatment of the dynamics with intermediate nonlinearity given above is an approximation that is good as long as the nonlinearity does not become too big. For a better theoretical description of the regime $4J < U < E_{\text{gap}}$, techniques developed in the field of nonlinear physics (e.g., nonlinear optics discussed in Sec. V.F) can be applied.

In the work of Louis *et al.* (2003) and Ahufinger and Sanpera (2005) it becomes clear that although solitonic solutions do exist, they exhibit structure on the length scale of the periodicity, which in the discussion thus far has not been included. Additionally, the solitonic solutions can be classified in terms of their symmetry with respect to the minima of the periodic potential. A set of solutions found by Louis *et al.* (2003) is depicted in Fig. 11.

A further feature of these discrete solitons is their reduced mobility due to the Peierls-Nabarro barrier (Ahufinger *et al.*, 2004). This barrier can be understood by looking at two extreme situations for a moving discrete soliton. If the initial condition of the propagation is described by an antisymmetric excitation [see Fig. 11(b)], i.e., the center of the envelope coincides with a maximum of the periodic potential, a moving soliton implies that at a certain time later the envelope will be symmetric [see Fig. 11(a)]. It follows directly from the results shown in Fig. 11 that this motion can only be excited if the kinetic energy overcomes the difference in chemical potentials for these two collective excitations. This barrier is essential for the-formation of stable solitons in two dimensions (Kalosakas *et al.*, 2002; Efremidis

et al., 2003; Ostrovskaya and Kivshar, 2003, 2004b; Ahufinger *et al.*, 2004) which are *not* stable in the weak potential limit (Baizakov *et al.*, 2002). This instability can be eliminated by applying a time-dependent nonlinearity or time-dependent dispersion (Abdullaev *et al.*, 2003).

The situation $E_{\mathrm{gap}} < U < 4J$ implies the weak potential limit and it makes clear that the dynamics cannot be described within a single band approximation anymore. In this regime, the linear concept of a band structure does not even allow for qualitative predictions and only concepts of nonlinear physics lead to reasonable results.

Generally one can state that in the regime of intermediate nonlinearity it is very difficult to find analytical solutions since all energy scales involved are of comparable magnitude. Thus the usual simplifying approach of neglecting terms associated with energy scales much smaller than the characteristic energy scale cannot be applied.

D. Nonlinear energy scale is dominant

This regime implies that the nonlinear on-site interaction energy is even larger than the gap energy. The concept of a linear band is, therefore, no longer suitable. First of all, we discuss the description employing the concept of an effective potential, which is obtained by using perturbation theory. This leads to a very simple description of the dynamics in this regime. Subsequently, we present the quite surprising fact that in this regime even *analytical* solutions exist. Finally, we present the energies of stationary solutions as a function of the quasimomentum, which reveal interesting loop structures in the regime discussed here.

1. Effective potential approximation

The basic idea of this approach is to describe the motion of each atom in an effective potential given by the sum of the external periodic potential and the energy variation due to the $|\Psi|^2$ term in the Gross-Pitaevskii equation. Since in the case of a periodic potential the atomic density is highest at the potential minima, the potential energy will be effectively reduced (increased) due to the repulsive (attractive) atom-atom interaction. Choi and Niu (1999) derived an explicit analytic expression for the effective potential using perturbation theory, leading to

$$V_{\mathrm{eff}} = \frac{V_0}{1+4C}\cos^2(kx) + \mathrm{const}, \tag{38}$$

with $C = \pi n_0 a / k^2$ which is the nonlinear energy U for the homogeneous case in units of $8E_R$. This result is a good approximation as long as the condensate density is nearly uniform, which is the case for weak external potentials or strong atomic interaction.

Within this approximation it was predicted that the motion of a homogeneous Bose-Einstein condensate in a periodic potential for dominating nonlinearity is hardly changed due to the presence of the periodic potential. Furthermore, an increase in the Landau-Zener tunneling probability was first suggested by Choi and Niu (1999) and studied in more detail by Liu *et al.* (2002). This increase in tunneling probability can be understood straightforwardly by realizing that in the case of repulsive atom-atom interaction the modulation of the effective potential is smaller than in the linear case and thus the gap energy is also smaller.

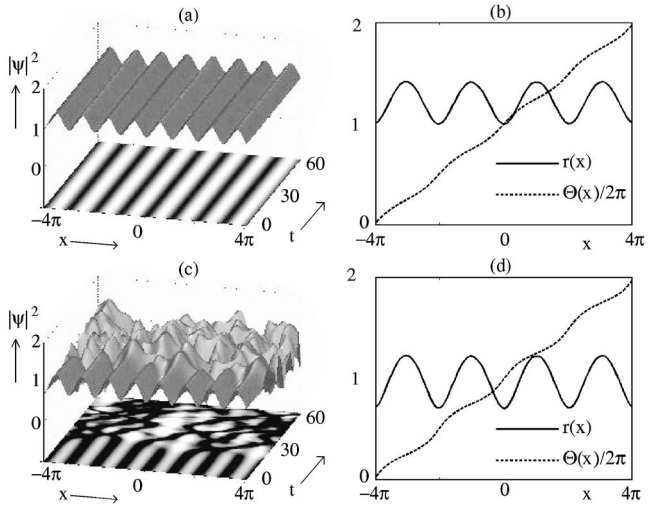

FIG. 12. Evolution of perturbed trigonometric solutions ($k=0$) with nontrivial phase (Bronski *et al.*, 2001a). (a),(c) The temporal dynamics of a stable and unstable solution, respectively. The difference of the initial conditions is shown in (b),(d), where r represents the absolute square value and θ the phase of the initial wave function. The main difference is the constant background, which is smaller in the case of the unstable mode. Taken from Bronski *et al.*, 2001a.

2. Analytic stationary solutions

Although most of the solutions in the regime we discuss here cannot be derived analytically, there is one special case for which a class of analytical solutions can be given. This is the homogeneous case, i.e., without an additional external potential. Bronski *et al.* (2001a, 2001b) derived the solution for a potential of the form $V(x) = -V_0 \mathrm{sn}^2(x,k)$, where $\mathrm{sn}(x,k)$ denotes the Jacobian elliptic sine functions with the elliptic modulus $0 \leqslant k \leqslant 1$. In the limit of $k=0$, the potential is sinusoidal and thus describes the case of an optical lattice.

The main result is that there exist stationary solutions with and without a nontrivial phase. One set of solutions with a nontrivial phase is shown in Fig. 12 for the case of $k=0$ corresponding to a sinusoidal potential. As one can see, the stability of the solutions depends on the background density of atoms. If the background is below a critical value, the solution becomes unstable. This behavior will be discussed in more detail in Sec. V.E on stability. This is another example of the striking phenomena one encounters in nonlinear physics—nonlinearity leads to *instability* in the first place, but by adding a constant background of atoms leading to a ho-

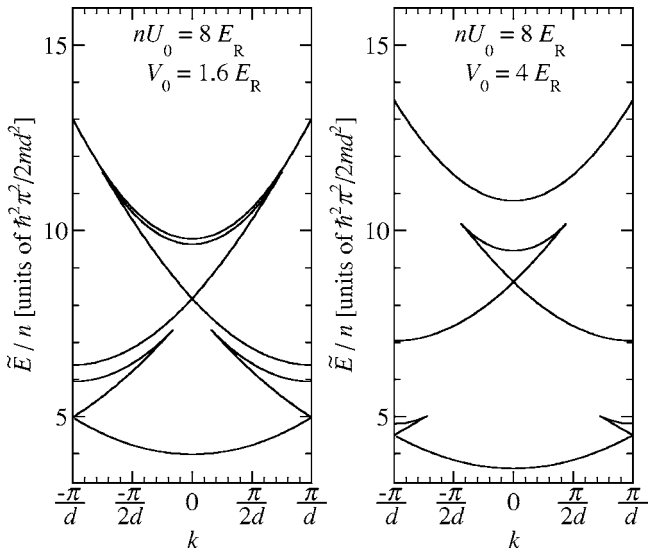

FIG. 13. Energy per particle as a function of the quasimomentum (Machholm *et al.*, 2003). The energy spectrum can be interpreted as a modified linear band structure. Significant modifications are observed for quasimomenta at which two bands of the linear system come close to each other. The structure becomes less pronounced when the potential modulation is increased (right graph).

mogeneous nonlinear energy the solutions can be *stabilized*.

3. Loops in the band structure

When the nonlinear on-site interaction energy is larger than the gap energy, one cannot expect the linear concept of band structure to be applicable. Nevertheless, the solutions of the nonlinear problem that minimize the energy still reveal some connection to the linear band structure, although new features such as loops come into play (see Fig. 13).

The first indications of the appearance of loops were found by Wu and Niu (2000) who investigated a two-mode model. They showed that for large nonlinearity ($U > E_{\mathrm{gap}}$) instabilities appear in the band structure near the boundary of the first Brillouin zone. Further works more clearly revealed nonanalytic behavior at the zone boundary (Wu *et al.*, 2002; Wu and Niu, 2003), as discussed in detail by Diakonov *et al.* (2002). In Fig. 13, two numerically calculated energy spectra are shown that reveal a swallowtail shape near the center and the edge of the Brillouin zone.

Although loops seem to be a feature of the periodic potential, Machholm *et al.* (2003) discuss that for the center of the Brillouin zone they are a general phenomenon that even persists in the limit of vanishing periodic potential. In the zero potential limit, the loop formed between the second and third bands becomes degenerate with a very special excited state of a condensate, namely, a train of dark solitons.

The connection of the appearance of the loop structure with superfluidity and hysteretic behavior was discussed by Mueller (2002). The loop structure appears because the energy landscape has two local minima (corresponding to the lower part of swallowtail and the normal band) separated by a state corresponding to a local maximum of the energy (upper part of the swallowtail).

Although finding stationary solutions is very important, in the laboratory one will only actually see solutions that are also stable against perturbations. Therefore, a thorough stability analysis of the solutions is necessary to make a direct connection between theory and possible experiments.

E. Stability analysis

The analysis of the stability of solutions in nonlinear systems is essential. In the context of periodic potentials, two classes of instabilities can be identified: *Landau/energetic instabilities*, for which small perturbations lead to a lowering of the systems's energy, and *dynamical/modulational instabilities*, for which small perturbations grow exponentially (Wu and Niu, 2000, 2001, 2002, 2003; Burger *et al.*, 2002; Wu *et al.*, 2002; Machholm *et al.*, 2003).

1. Landau (energetic) instability

Landau instability is often discussed in the context of Bose liquids and their remarkable property of superfluidity, i.e., a liquid flows through capillaries or other types of tight spaces without friction if its speed is below a critical value. Landau argued that a quantum current suffers friction only when the creation of excitations (phonons) on the liquid lowers the energy of the quantum system. The same is true for a Bose-Einstein condensate in the presence of an optical lattice.

In order to find out whether small excitations lower the energy of a given Bloch state $e^{iqx}\phi_q(x)$, one calculates the energy of a slightly perturbed Bloch state given by

$$\Psi_q(x) = e^{iqx}[\phi_q(x) + u_q(x,Q)e^{iQx} + v_q^*(x,Q)e^{-iQx}]. \tag{39}$$

The functions $u_q(x,Q)$ and $v_q^*(x,Q)$ have the same period as the periodic potential and $Q \in [-\pi/d, \pi/d]$. The energy deviation due to the perturbation can be found by evaluating the expectation value of the energy given in Eq. (11) with the mean-field approximation. A detailed discussion of the mathematical method is given in Berg-Sørensen and Mølmer (1998), Machholm *et al.* (2003), and Wu and Niu (2003).

If the energy of the perturbed Bloch state increases, the original Bloch wave corresponds to a local energy minimum and thus exhibits superflow. In the situations for which δE is negative, normal flow is expected. Since the general situation of an arbitrary initial Bloch wave is very complicated and not solvable analytically, numerical calculations are necessary. The results are summarized in the stability phase diagram shown in Fig. 14.

The physical situation is defined by three parameters: the potential modulation depth V_0, the nonlinearity U_n, where n is the mean density and U is defined in Eq. (29)

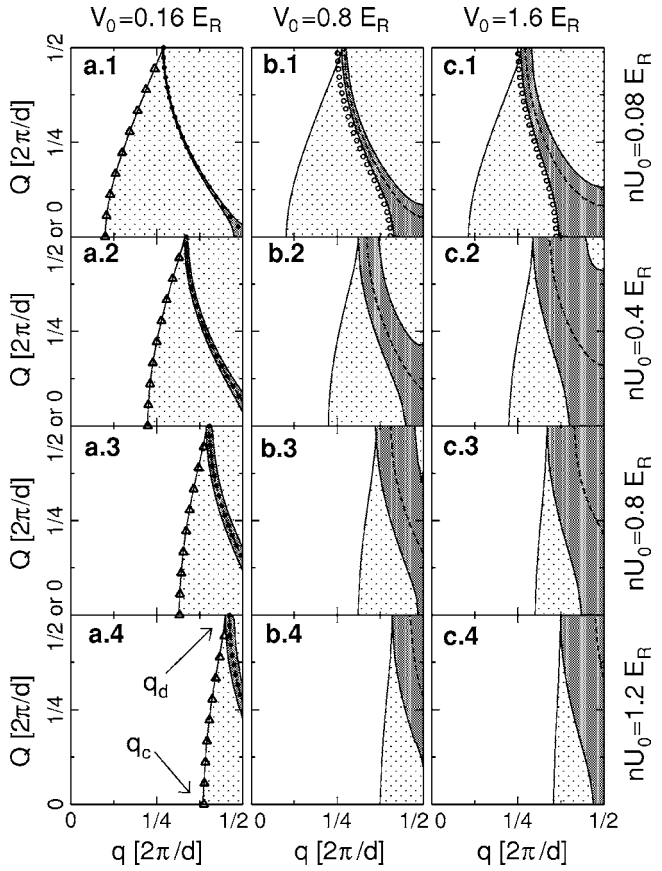

FIG. 14. Stability diagram obtained by Wu and Niu (2001). The parameters describing the physical situation are the potential modulation V_0, the nonlinearity nU for the homogeneous case, and the quasimomentum of the homogeneous condensate (flow of the condensate). The parameter Q is the corresponding wave vector of the perturbation. It is important to note that $Q=\pi/d$ implies a modulation of the density with twice the period of the periodic potential. The regime in which the stationary states exhibit a Landau instability are indicated by the light shaded area and associated critical quasimomentum q_e. The dark shaded area represents the dynamically unstable regime with associated critical quasimomentum q_d.

assuming a homogeneous wave function, and the quasimomentum q corresponding to the flow of the homogeneous Bose-Einstein condensate. For each parameter the energy deviation δE is calculated as a function of the free parameter $Q=\pi/D$, which describes a perturbation with the spatial period D. The light shaded area in Fig. 14 represents the Landau unstable region in which the system's energy can be lowered by emitting phonons.

If the quasimomentum of the Bose-Einstein condensate q is slowly increased, the first excitation modes which can lower the energy have very long wavelength $Q\rightarrow 0$ and occur when $q=q_e$. Machholm *et al.* (2003) systematically explore the dependence of q_e on the nonlinearity and on the potential modulation depth. The onset condition of these long-wavelength instabilities can be obtained analytically by the hydrodynamic approach already discussed (Krämer *et al.*, 2003; Menotti *et al.*, 2003b).

2. Dynamical instability

One unique feature of Bose-Einstein condensates in optical lattices is the occurrence of *dynamical instability*, which in a homogeneous system is only present for attractive interactions but can be induced by the presence of a periodic potential even when the interactions are repulsive. Dynamical instability implies that small deviations from the stationary solution grow exponentially in time.

The analysis is analogous to the energetic instability analysis, but now the modified state is inserted into the *time-dependent* Gross-Pitaevskii equation. By keeping only the linear term in the perturbation, one ends up with linear differential equations describing the time evolution of the small perturbation (Machholm *et al.*, 2003; Wu and Niu, 2003).

If the corresponding eigenvalues are real, the Bloch state is stable. Complex eigenvalues, however, indicate that the perturbation will grow exponentially. The results obtained by Wu and Niu (2003) are given in Fig. 14 with the dark shaded areas. It is important to note that dynamical instability can only occur for Bloch states that are also energetically unstable. The mode that becomes unstable for the quasimomentum of the condensate $q=q_d$ is specified by $Q=\pi/d$. This implies that the corresponding exponentially growing mode represents a period doubling (Machholm *et al.*, 2004), since the functions $u(x)$ and $v(x)$ in Eq. (39) have the same period as the periodic potential. A very general discussion of dynamical instabilities for weakly interacting many-body systems is given by Anglin (2003)

A systematic analysis giving the quasimomentum q_e and q_d for the onset of the energetic and dynamic instabilities, respectively, as a function of potential depth and nonlinearity can be found in Machholm *et al.* (2003). It is important to note that in the discussion so far we have always assumed a one-dimensional situation. As already stated at the very beginning, most of the experiments carried out to date have not been in this regime. Only recently has the instability analysis been extended to more realistic cases by taking into account the transverse degrees of freedom (Modugno *et al.*, 2004).

There have also been investigations of dynamical instability in the context of an effective-mass approximation. In this case one also speaks of a "modulational instability," which is well known in the field of nonlinear optics. It has been shown that within this approximation the stability of the Bloch waves at the band differs dramatically between the lower and upper bands (Konotop and Salerno, 2002). While the modes in the lower band are unstable due to the negative mass, the lower edge of the first excited band is stable, as one would expect from the positive effective mass. It is important to note that a negative mass (deduced from the linear theory) is only a sufficient criterion for instability, but not necessary.

F. Analogy to nonlinear optics

Many of the effects discussed so far have already been treated in the field of nonlinear photon optics. There is a

TABLE II. Translation between the notation in the BEC community and the nonlinear optics community. Here we only specify the limit of weak periodic potentials and Bragg-grating fibers.

Light optics		Atom optics
t,x	$\leftrightarrow$	x,t
β	$\leftrightarrow$	$\hbar/m_{\mathrm{eff}}$
γ	$\leftrightarrow$	$2\alpha_{\mathrm{nl}}a\omega_{\perp}$

direct connection between Bose-Einstein condensates in periodic potentials and the physics of intense laser pulses in spatially modulated refractive index structures exhibiting a Kerr nonlinearity (Agrawal, 2001). In optics the refractive index modulation can be realized in the direction of the propagation of the laser pulse by Bragg fibers [Eggleton and Slusher (1996); for an overview, see deSterke and Sipe (1994)], which is the optical analog of the weak periodic potential limit discussed in Sec. V.B. The equation describing the propagation of the envelope A of an intense laser pulse is given by (Agrawal, 2001)

$$i\frac{\partial A}{\partial x}=\frac{1}{2}\beta\frac{\partial^2 A}{\partial t^2}-\gamma|A|^2A. \tag{40}$$

The relevant parameters are the group velocity dispersion parameter β and the nonlinearity parameter γ. Thus the results obtained in the optical regime can be directly transferred to the atomic system by using Table II.

By realizing weakly coupled optical wave guide arrays [for an overview, see Christodoulides *et al.* (2003)] one has the optical analog of the deep potential limit discussed in Sec. V.B.2. The main advantage of the atomic system lies in the fact that very large nonlinearities can be realized that are not accessible in optical systems.

G. The Bose-Hubbard model

In the preceding discussion of the theoretical treatment of Bose-Einstein condensates in periodic potentials, we have distinguished different regimes depending on the relative importance of the nonlinear interaction and the lattice parameters. In all these regimes, however, our starting point was the Gross-Pitaevskii equation treating the condensate as a classical field. When the number of atoms per lattice well becomes small, however, the "granular structure" of the condensate starts being important and particle correlations need to be taken into account properly. For this regime, Jaksch *et al.* (1998) suggested using the Bose-Hubbard model originally conceived for superfluid He in restricted geometries [such as Vycor, or other porous media; see Fisher and Weichman (1989)]. As a number of important recent experiments with BECs in lattices operated in this regime (see Sec. VI.E.3), we give here a brief summary of the theoretical approach.

For a condensate confined in the combined potential of an optical lattice and a harmonic trap, the Bose-Hubbard Hamiltonian can be written as (Zwerger, 2003)

$$\hat{H}=-J\sum_{\langle ll'\rangle}\hat{b}_l^{\dagger}\hat{b}_{l'}+\frac{U}{2}\sum_l\hat{n}_l(\hat{n}_l-1)+\sum_l\varepsilon_l\hat{n}_l, \tag{41}$$

where $\langle ll'\rangle$ denotes the sum over nearest-neighbor pairs (with double counting), and ε_l is the energy at site l associated with the harmonic trapping potential. In this equation, $\hat{b}_l^{\dagger}$ and $\hat{b}_l$ are the destruction and creation operators for a boson at lattice site l, respectively, and $\hat{n}_l$ denotes the number operator for site l. This Hamiltonian supports a zero-temperature quantum phase transition between superfluid and insulating phases controlled by the ratio U/J of the on-site interaction and tunneling energies. Intuitively, one can understand what happens at the critical value $(U/J)_c$ by considering N atoms in a lattice with $M=N$ sites: When the tunneling between adjacent sites is sufficiently small, hopping events that increase the on-site energy because of multiple occupancy of a single site are suppressed, and the system assumes the lowest energy state. This corresponds to having exactly one atom per lattice site, and the overall wave function in the Mott insulator state is simply the product of the corresponding local Fock states.

A more thorough analysis (Zwerger, 2003) reveals that Mott insulator phases exist also for $\bar{n}=2,3,4,\ldots$ atoms per lattice site. For two- and three-dimensional lattices, it can be shown that the critical value for U/J is given by

$$(U/J)_c=5.8z \text{ for } \bar{n}=1,\ (U/J)_c=4\bar{n}z \text{ for } \bar{n}\gg 1, \tag{42}$$

where z is the number of nearest neighbors. In one dimension, increased quantum fluctuations lead to deviations from these formulas, giving $(U/J)_c=2.2\bar{n}$ for large $\bar{n}$ and $(U/J)_c=3.84$ for $\bar{n}=1$.

Furthermore, the Bose-Hubbard model has also been used to make predictions about Bloch oscillations in the regime where atom number fluctuations are crucial (Kolovsky, 2003). Recently, it has been worked out that there is a close connection between quantum chaos and irreversible decay of Bloch oscillations in the context of the Bose-Hubbard model (Buchleitner and Kolovsky, 2003).

VI. EXPERIMENTS

In the following two sections, we give an account of the experimental studies to date on BECs in optical lattices. We focus mainly on those experiments that are relevant to the theoretical discussion of the previous sections. In a number of other experiments, interfering laser beams were used mainly as a tool to probe properties of the condensate on its own. Some of these experiments will be discussed briefly in Sec. VI.F.

A. Detection and diagnostics

Doing experiments with condensates in optical lattices is useful only if one is able to extract information from the system once the experiment has been carried out. As with BECs in harmonic traps (see Sec. II), there are essentially two methods for retrieving information from the condensate: *in situ* and after a time of flight. In the former case, one can obtain information about the spatial density distribution of the condensate, its shape, and any irregularities on it that may have developed during the interaction with the lattice. Also, the position of the center of mass of the condensate can be determined.

Looking at a condensate released from a lattice after a time of flight (typically on the order of a few milliseconds) amounts to observing its momentum distribution.[15] A harmonically trapped condensate has a Gaussian momentum distribution in the limit of small interactions, whereas in the Thomas-Fermi limit (in which the interactions dominate over the kinetic energy contribution) it has a parabolic density profile and expands self-similarly after being released. By contrast, a condensate in a periodic potential contains higher momentum contributions in multiples of $2\hbar k_L$, their relative weights depending on the depth of the lattice. In fact, in the tight-binding limit (see Sec. IV) we can consider the condensate to be split up into an array of local wave functions that expand independently after the lattice has been switched off. Eventually they all overlap and form an interference pattern that (in the absence of interactions) is the Fourier transform of the initial condensate. In the case of a very elongated (along the lattice direction) condensate, to a good approximation we initially have an array of equally spaced Gaussians of a width $\ll d$ determined by the lattice depth. Since such an array can be written as the convolution of a single Gaussian wave function with a comb of δ functions with spacing d, the Fourier transform of this object is simply the product of the individual transforms, i.e., another array of δ peaks multiplied by a Gaussian that determines the relative heights (intensities) of the peaks.

Figure 15 shows a typical time-of-flight interference pattern of a condensate released from an optical lattice (plus harmonic trap) for a lattice depth $V_0 \approx 10E_R$. From the spacing of the interference peaks and the time of flight, one can immediately infer the recoil momentum of the lattice and hence the lattice constant d. Furthermore, from the relative height of the side peaks corresponding to the momentum classes $\pm 2\hbar k_L$, one can calculate the lattice depth (see Sec. VI.B).

So far, we have assumed that the local wave functions in the lattice wells have the same phase (or differ by a constant). If this is no longer true, i.e., if there are random phase differences between adjacent lattice sites, the interference pattern becomes less distinct. Depending on the nature and magnitude of the phase differences, the appearance of the interference pattern can range from a slight broadening of the peaks to their complete disappearance. The degree of the "smearing out" of the interference pattern can be quantified through the following parameters (see Fig. 16):

(i) The *visibility*, defined in analogy with interferometry as the normalized difference between the maxima $h_{\max}$ and minima $h_{\min}$ of an interference pattern, i.e.,

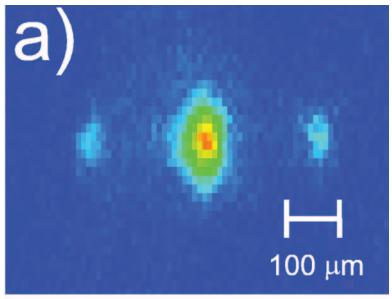

FIG. 15. (Color) Interference pattern of a Bose-Einstein condensate released from a one-dimensional optical lattice of depth $V_0=10E_R$ after a time of flight of 20 ms. In (a), the lattice was at rest, whereas in (b) it had been accelerated to v_R, i.e., the quasimomentum of the condensate was at the edge of the Brillouin zone.

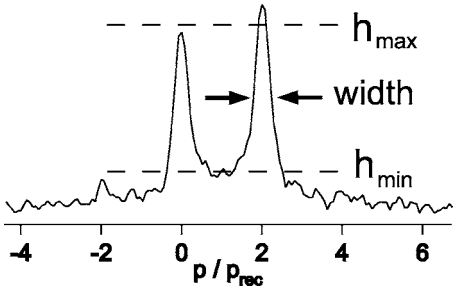

FIG. 16. Quantities used to characterize the interference pattern of a condensate released from an optical lattice. Shown here is an absorption image integrated perpendicular to the lattice direction. Similarly to Fig. 15, the condensate was accelerated to the edge of the Brillouin zone before being released. The x axis of this figure has been rescaled (in units of the recoil momentum $p_{\mathrm{rec}}=mv_R$) to reflect the condensate momentum before the release from the lattice.

[15]Note that after the lattice is switched off, s-wave collisions between condensate atoms can lead to deviations from this idealized picture. In fact, for high densities s-wave spheres can be visible in the time-of-flight picture, leading to a reduced contrast of the interference pattern.

$$V = \frac{h_{\max} - h_{\min}}{h_{\max} + h_{\min}}. \tag{43}$$

(ii) The *width of the peaks*, which reflects the effective number of wells that contribute coherently to the interference pattern. If all condensates are in phase, this width reaches a minimum that is directly related to the finite number of wells $\mathcal{V}$ occupied by the condensate, i.e., the width is proportional to $1/\mathcal{V}$.

When interpreting the results of measurements of the visibility or the peak width of an interference pattern, care must be taken in order to understand properly the origin of a possible variation in these quantities. In fact, contrary to intuition, even an array of condensates whose phases are completely independent and, therefore, uncorrelated can exhibit a clear interference pattern after a time of flight (Hadzibabic *et al.*, 2004), albeit with a fluctuating longitudinal position and modulation depth.

B. Calibration of optical lattices

In the following discussion of experiments with condensates in lattices, we often quote lattice depths (in units of the recoil energy E_R), and we have to worry about how and with what precision these can be measured. Especially in experiments in which the agreement with theory depends critically on an exact knowledge of the lattice depth (e.g., when the tunneling rate, which depends exponentially on the depth, is involved), it is important to have a reliable tool for calibrating the experiment.

In principle, the lattice depth can be calculated from Eq. (6) if one knows the saturation intensity of the atomic transition and the parameters of the lattice beams, i.e., their waists, detunings, and powers. While the atomic polarizability is usually well known for the atomic species typically used in lattice experiments, and the detuning of the lattice laser can be measured with great accuracy by using spectroscopy, the waist and power of the beam (and hence its intensity at the position of the condensate) are more difficult to measure. Even if the waist is accurately measured at some point along the optical path of the lattice beam, further propagation and passage through the windows of the vacuum system can distort the beam and lead to deviations from the calculated intensity profile. Absolute optical powers, on the other hand, are notoriously difficult to measure, resulting in combined systematic errors on the order of 10–20 % or more.

Measuring the magnitude of a well-understood effect of the optical lattice on the atoms will, therefore, lead to more precise values of the lattice depth. It is important, however, to make sure that the density of the condensate is sufficiently low so that mean-field effects that could influence the result are minimized. This can be achieved by either choosing a small harmonic trapping frequency or by releasing the condensate from the trap and allowing it to expand slightly before doing the measurement. With this proviso, we now list the methods typically used to calibrate optical lattices:

(i) *Rabi oscillations (Pendellösung)*. By suddenly switching on a lattice moving at v_R, the condensate is loaded into a coherent superposition of population in the ground state and the first excited band. The relative phases of the populations and hence the weights of the 0 and $2\hbar k_L$ momentum components (measured after a time of flight) evolve with frequency $\Omega_{\mathrm{Rabi}} = V_0/2\hbar$ in the shallow lattice limit, from which V_0 can be calculated (Ovchinnikov *et al.*, 1999).

(ii) *Raman-Nath diffraction*. If the lattice is switched on suddenly for a time $\Delta t \ll 1/\omega_{\mathrm{rec}}$, the resulting diffraction pattern is in the Raman-Nath regime and the value of V_0 can be calculated from the relative populations in the 0 and $\pm 2\hbar k_L$ momentum components (Gould *et al.*, 1986). This method has the advantage of needing only a short interaction time with the lattice.

(iii) *Expansion from the lattice*. In this method, one loads the condensate adiabatically into the lattice (see below) and then switches off the lattice lasers. The diffraction pattern observed after a time of flight is the product of a series of momentum peaks of spacing $2v_R t_{\mathrm{TOF}}$ and a Gaussian envelope whose width reflects the localization of a local wave packet in a lattice well. From the relative weight $P_{\pm 1}$ of the 0 and $\pm 2\hbar k_L$ momentum peaks, the lattice depth can be calculated from

$$s = \frac{16}{[\ln(P_{\pm 1})]^2} P_{\pm 1}^{1/4} \tag{44}$$

in the limit of deep lattices ($s \gtrsim 5$) (Cristiani *et al.*, 2002).

(iv) *Landau-Zener tunneling*. As described in Sec. IV.B.3, if the lattice is accelerated across the edge of the Brillouin zone, Landau-Zener tunneling occurs with a probability $r = \exp(-a/a_c)$ in the shallow lattice limit, for which the energy gap at $q = \hbar k_L$ is roughly half the lattice depth.

(v) *Parametric heating*. By periodically modulating the depth of the optical lattice, the condensate atoms can be parametrically excited (Friebel *et al.*, 1998). If the modulation frequency is equal to twice the harmonic trapping frequency in the lattice wells, heating will occur. From this resonant modulation frequency, the lattice depth can be calculated via Eq. (8).

C. Preparation of a Bose condensate in an optical lattice

In order to do experiments with Bose condensates in optical lattices, one first has to create such a condensate.

There are two possibilities to do this: one either first creates a BEC in a conventional harmonic (magnetic or optical) trap, and then adiabatically adds the periodic potential, or else one performs evaporative cooling with the periodic potential already present and reaches condensation in the combined trap.

The latter of these approaches was pioneered by the Florence group (Burger *et al.*, 2001) and uses a conventional protocol for evaporative cooling in a magnetic trap down to temperatures just above the threshold for Bose-Einstein condensation. At this point, the optical lattice potential is switched on and evaporative cooling continues. In this way, the system condenses directly into the ground state of the harmonic plus periodic potential. The use of this method presupposes that the optical lattice is sufficiently far-detuned so that during the time needed for evaporative cooling (on the order of a few seconds) with the lattice present no photons are scattered that could disturb the condensate.

The alternative approach, namely, adding the periodic potential once condensation has occurred, requires some careful thought as to the conditions for adiabaticity. If the condensate density is low and the mean-field interaction is negligible, the adiabaticity criterion follows straightforwardly from the band structure of the BEC in the lattice. Essentially, in order to end up with the condensate in the lowest energy band of the lattice, one has to switch on the lattice lasers sufficiently slowly in order to avoid excitation into higher bands. This consideration leads to an adiabaticity criterion for loading into a single Bloch state $|n,q\rangle$ of the form (Denschlag *et al.*, 2002)

$$\left|\left\langle i,q\left|\frac{\partial H}{\partial t}\right|0,q\right\rangle\right| \ll \Delta E^2(q,t)/\hbar, \tag{45}$$

where ΔE is the energy difference between the ground state and the first excited state $|i\rangle$. Typically, the lattice is at rest in the lab frame when switched on, i.e., $q=0$. In this case, it can be shown that the adiabaticity criterion Eq. (45) is satisfied if $dV_0/dt \ll 16\, E_R^2/\hbar$. For typical potential depths of a few E_R and a recoil energy $E_R=h \times 3.7$ kHz (for Rb atoms), one finds that switching on the lattice linearly from 0 to its full depth in more than 1 ms should ensure adiabaticity. A method for circumventing this adiabaticity criterion while still loading the condensate entirely into the lowest energy band is described in Mellish *et al.* (2003).

When $q \neq 0$, i.e., the lattice is moving while it is being ramped up, the adiabaticity criterion becomes more and more difficult to satisfy as the distance between the ground state band and the first excited band shrinks with increasing q. In fact, at the edge of the first Brillouin zone, where $q=1$, it is impossible to load the condensate into the ground state band as the latter is degenerate with the first excited band when $V_0=0$. If the lattice is switched on suddenly with $q=1$, the two lowest energy bands are equally populated, leading to Rabi oscillations that can, e.g., be used to calibrate the lattice depth (see Sec. VI.B).

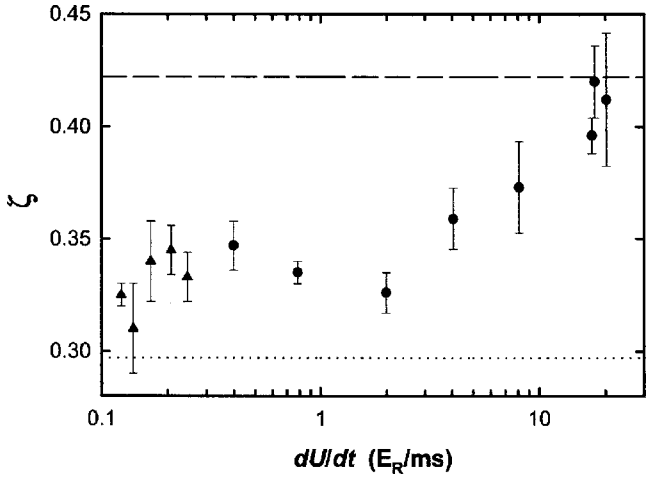

FIG. 17. Adiabaticity of the loading process. The faster the potential is ramped up, the larger the parameter ζ (ratio of the width of the interference peaks to the separation of the peaks) describing the dephasing of the condensate (from Orzel *et al.*, 2001).

Loading the condensate adiabatically into the lattice for $\hbar|q|>1\hbar k_L$ is also possible. In this case the quasimomentum lies outside the first Brillouin zone and the condensate will, therefore, not end up in the lowest energy band but in one of the excited bands. For instance, loading the condensate into a lattice with $\hbar q=1.5\hbar k_L$ means (assuming adiabaticity) populating the state $|n=1,\hbar q=-0.5\hbar k_L\rangle$ where the quasimomentum has been projected back into the first Brillouin zone. This follows from the conservation of energy and momentum and has been verified experimentally in both cold atoms (Dahan *et al.*, 1996) and BECs (Jona-Lasinio *et al.*, 2003).

In both the ground state and excited state bands it is possible to change the quasimomentum of the condensate after loading by accelerating the optical lattice. By applying a known acceleration a for a certain time, any value of q can be selected. Care must be taken to chose a sufficiently small value for a if the edge of the Brillouin zone is to be crossed, as otherwise Landau-Zener tunneling can occur. If the condensate is to be kept at the final q for some time, the lattice must keep moving at the velocity it reached at the end of the acceleration. In this case, the restoring force of the harmonic potential in which the condensate is held must be taken into account if the spatial movement of the condensate during the interaction time with the lattice is appreciable.

If the condensate density is sufficiently large for the mean-field interaction to be important, a new energy scale enters the problem. One now has to consider the lowest-lying phonon modes that can be excited in the condensate (Javanainen, 1999; Orzel *et al.*, 2001). The lower the ramping speed, the less the condensate is "disturbed" by the lattice. This can be quantified by measuring the width of the interference peaks as a function of the ramping speed (see Fig. 17). Conversely, one can observe the effects of a deliberately *nonadiabatic* ramping

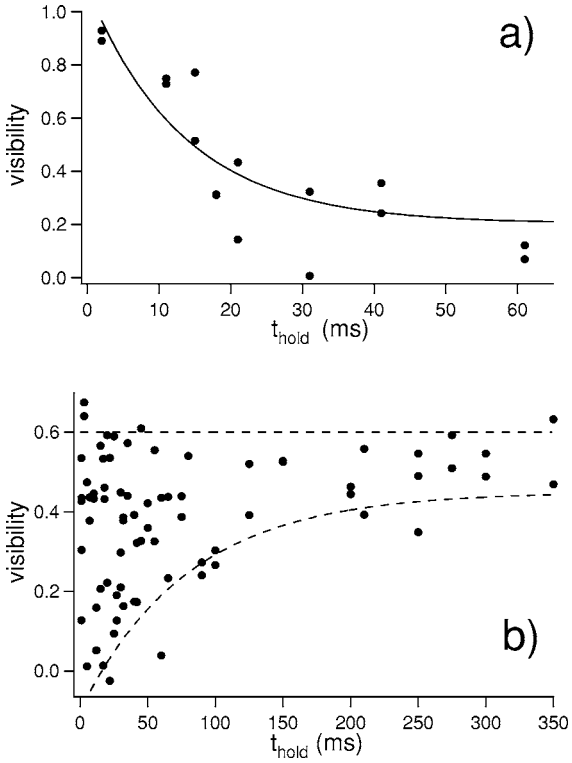

FIG. 18. Initial dephasing (a) and eventual rephasing (b) of a condensate nonadiabatically loaded into an optical lattice. In this experiment, the criterion describing the phase coherence of the condensate is the visibility of the interference pattern [from Morsch *et al.* (2003b)]. Note that (a) and (b) refer to different harmonic trapping frequencies, leading to different time scales for dephasing.

of the lattice depth[16] by looking at the interference pattern after the condensate was released from the trap. Morsch *et al.* (2003a, 2003b) observed that, after an initial washing out of the interference peaks due to dephasing of adjacent lattice wells through the different local mean-field energies (see Fig. 18), phase coherence was restored on the time scale of interwell tunneling (≈200 ms for their experimental parameters), but at the expense of a decrease in the condensate fraction. In Fig. 18(b), the rephasing is indicated by the lower envelope of the scattered visibility points, showing that after the initial dephasing the shot-to-shot fluctuations of the visibility decrease as condensates in adjacent lattice wells regain a stable phase relationship.

D. Experiments in shallow lattices

1. Bloch oscillations and Landau-Zener tunneling

The formal resemblance between electrons in crystals and BECs in optical lattices inspired a number of experiments that probed their band structure and interband tunneling properties. The most striking effect of the band structure of periodic potentials, namely, the occurrence of Bloch oscillations and Landau-Zener tunneling when a constant force is applied to the atoms, had already been observed in ultracold atoms before condensates entered the scene (Dahan *et al.*, 1996; Niu *et al.*, 1996). Bose-Einstein condensates, however, offered the possibility to investigate them more systematically and in different regimes. The first experiment along these lines with Bose condensates in optical lattices was carried out by Anderson and Kasevich (1998), sparking considerable interest in both the theoretical and experimental communities.

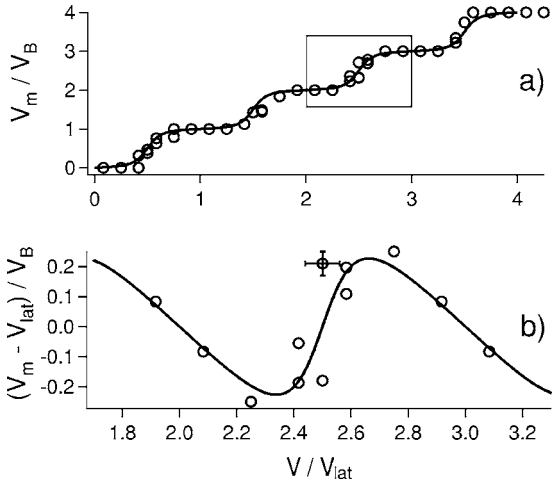

FIG. 19. Bloch oscillations (in momentum space) of a condensate in an optical lattice. If the instantaneous lattice velocity u_{lat} (indicated on the horizontal axis) is subtracted from the mean velocity of the condensate measured in the laboratory frame of reference (a), one clearly sees Bloch oscillations in the lattice frame (b). From Cristiani *et al.*, 2002.

a. Linear regime

In order to observe Bloch oscillations in the linear regime using a Bose-Einstein condensate, it is necessary to reduce its density sufficiently so that the mean-field term in the Gross-Pitaevskii equation becomes negligible. This can be achieved either by reducing the frequency of the magnetic trap, and hence the density of the condensate before switching on the optical lattice, or else by releasing the condensate from the magnetic trap and allowing it to expand. Morsch *et al.* (2001) carried out experiments in this regime, loading BECs of rubidium atoms into a shallow ($V_0 \approx 2E_R$) optical lattice that was subsequently accelerated with acceleration a by chirping the frequency difference between the lattice beams (Morsch *et al.*, 2001; Cristiani *et al.*, 2002). After a variable acceleration time t_{acc}, the trap and lattice were switched off and the condensate was observed after a time of flight. From the resulting interference pattern, the condensate group velocity in the frame of reference of the lattice could be calculated and plotted against the lattice velocity $u_{lat} = at_{acc}$ (see Fig. 19), clearly showing the Bloch oscillations.

[16] A theoretical analysis of this experiment can be found in Plata (2004).

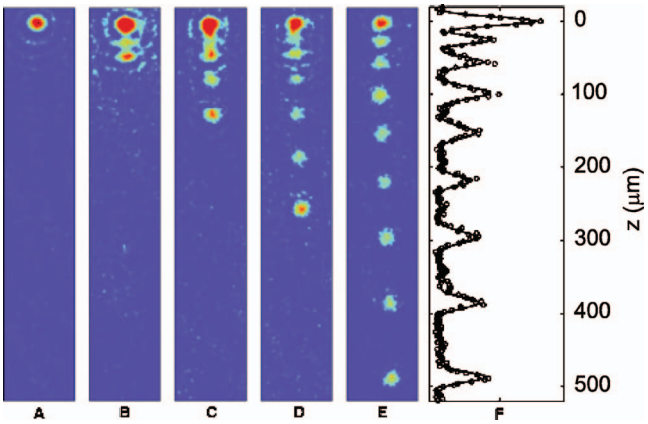

FIG. 20. (Color) Coherent "droplets" tunneling out of a condensate held in a vertical 1D optical lattice. This effect can be interpreted in terms of the condensate undergoing Bloch oscillations under the influence of the gravitational force and part of the condensate leaving the lattice due to Landau-Zener tunneling at successive crossings of the Brillouin zone edge. Holding times in the lattice are (a) 0, (b) 3, (c) 5, (d) 7, and (e) 10 ms, respectively. In (f), an integrated profile of the absorption image (e) is shown together with a theoretical fit (solid line). Taken from Anderson and Kasevich, 1998.

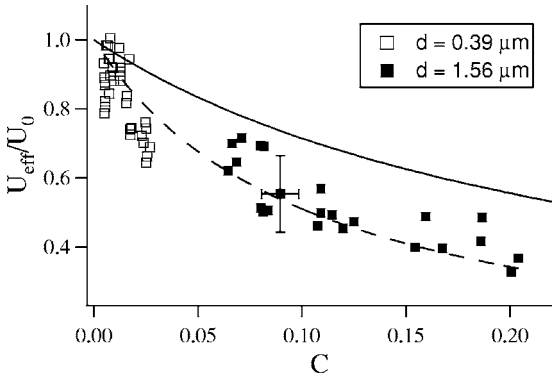

FIG. 21. Variation of the effective potential U_{eff} (corresponding to V_{eff} in the notation of this review) with the nonlinear parameter C. The square symbols are experimental data points (obtained by measuring the tunneling probability and using the linear Landau-Zener formula to infer an effective lattice depth, i.e., the equivalent lattice depth in the linear problem giving the experimentally measured tunneling probability), and the solid and dashed lines are the theoretical prediction by Choi and Niu (1999) and a best fit with a rescaled nonlinearity parameter, respectively. From Morsch *et al.*, 2001.

Another phenomenon occurring in an accelerated lattice is Landau-Zener tunneling, previously observed for ultracold atoms in a lattice (Niu *et al.*, 1996). When a is sufficiently large, the condensate cannot adiabatically follow the variation of energy with quasimomentum in the lowest band of the lattice. At the edge of the Brillouin zone ($q=1$), there is a finite probability r [given by Eq. (28)] for the condensate to tunnel into the first excited band, with the critical acceleration a_c given by Eq. (28). In the experiment by Anderson and Kasevich (1998), a vertically oriented lattice was used, with the Earth's acceleration g driving the atoms. The Landau-Zener tunneling events led to atomic "droplets" falling out of the lattice (see Fig. 20).

Another way of probing the band structure of a condensate inside an optical lattice is by coherently transferring population between the bands. This can be done either by shaking the lattice, i.e., periodically accelerating it forward and backward, or by modulating the lattice depth (Denschlag *et al.*, 2002). Starting with the condensate in the lowest energy band, the former method will transfer population into the first excited band, whereas in the latter case the second band will be populated. The transfer is most efficient if the modulation frequency matches exactly the energy separation between the two bands at the value of q chosen through the velocity of the lattice. Hence, by scanning q and finding the resonant modulation frequency in each case, one can map out the separation between two bands. If the q dependence of one of the bands is known, the other band can thus be reconstructed.

b. Nonlinear regime

When the nonlinear term in the Gross-Pitaevskii equation is not negligible any longer, the behavior of a BEC in an accelerated lattice deviates appreciably from the linear case (Morsch and Arimondo, 2002; Kolovsky, 2003). In particular, performing Landau-Zener tunneling experiments as a function of the nonlinear parameter C (see Sec. V.D.1), Morsch *et al.* (2001) found that the tunneling probability increased with increasing C. This can be explained in the effective potential approximation introduced by Choi and Niu (1999) as a decrease in the effective potential depth and hence the band gap at the Brillouin zone edge, leading to increased tunneling (see Fig. 21).

Interestingly, if the same experiment is carried out in the opposite direction, i.e., starting out with the condensate in the first excited band, the effect of the nonlinear term is exactly reversed. While in the linear case Landau-Zener tunneling from the lowest to the first excited energy band or vice versa occurs with the same probability, the mean-field interaction leads to an asymmetry in the tunneling. Jona-Lasinio *et al.* (2003) showed that in the nonlinear case one expects the tunneling probability from the first excited to the lowest band to be *reduced* rather than enhanced, as is the case for tunneling from the lowest to the first excited band. This asymmetry gets bigger as C increases and ultimately leads to a complete suppression of tunneling from the excited to the lowest energy band.

2. Instabilities and breakdown of superfluidity

In the previous section, we discussed a number of experiments in which the band structure of a BEC in a lattice was probed in the linear and nonlinear regimes. These experiments provide us with information about the eigenenergies of the Gross-Pitaevskii equation in the presence of a periodic potential, but they do not immediately reveal anything about the stability of the corre-

sponding wave functions. Such knowledge is important, however, if one wants to coherently manipulate a Bose condensate with an optical lattice. In Sec. V.E we discussed how a stability analysis can be carried out in theory and what kinds of instabilities one expects to encounter in the system we are dealing with. In this section, we look at the experimental results to date on instabilities in optical lattices.

In order to investigate instabilities experimentally, one first needs to find a measurable quantity that reflects this instability. For a Bose condensate in a lattice, the growth of an unstable mode will lead to a loss of phase coherence across the condensate which can be detected in a time-of-flight measurement. In Cristiani *et al.* (2004), a BEC was loaded into a lattice and subsequently accelerated up to a final velocity $v_{\text{final}} > v_R$, thus eventually crossing the edge of the Brillouin zone. The time-of-flight interference pattern was then characterized by its contrast (or visibility) as a function of the lattice acceleration. The latter determined the time the condensate spent in the quasimomentum region in which unstable modes are expected to be present. For small accelerations, beyond a critical quasimomentum the contrast of the interference pattern started to decrease, indicating the presence of unstable modes. In a similar experiment, Fallani *et al.* (2004) loaded the condensate into a lattice moving at a finite velocity and hence at a finite quasimomentum q (see Fig. 22). After a waiting time ranging from a few milliseconds up to several seconds, the condensate was imaged after a time of flight and the number of atoms in the condensate fraction was determined. Again, it was found that beyond a critical quasimomentum $q_{\text{crit}} \approx 0.55$ the condensate started to be "destroyed," i.e., atoms were lost from the condensed fraction. In contrast to Cristiani *et al.* (2004), this experiment investigates a single value of q at a time rather than an integrated effect over a range of quasimomenta.

Both of the experiments described above can be interpreted in terms of a dynamical instability arising above a critical quasimomentum and growing with a characteristic rate, as predicted by several authors (Machholm *et al.*, 2003; Wu and Niu, 2003). Although Fallani *et al.* (2004) and Sarlo *et al.* (2005) compare their results with numerical simulations, thorough and systematic measurements, e.g., of the growth rates of the unstable modes in different regions of parameter space (characterized by the lattice depth and the nonlinear parameter C) have yet to be done. An interesting prospect lies in the careful characterization of just *one* unstable mode[17] such as the period-doubling mode[18] theoretically discussed by Machholm *et al.* (2004). The need for more careful (and more quantitative studies) is highlighted by the difficulty in interpreting the experimental results and

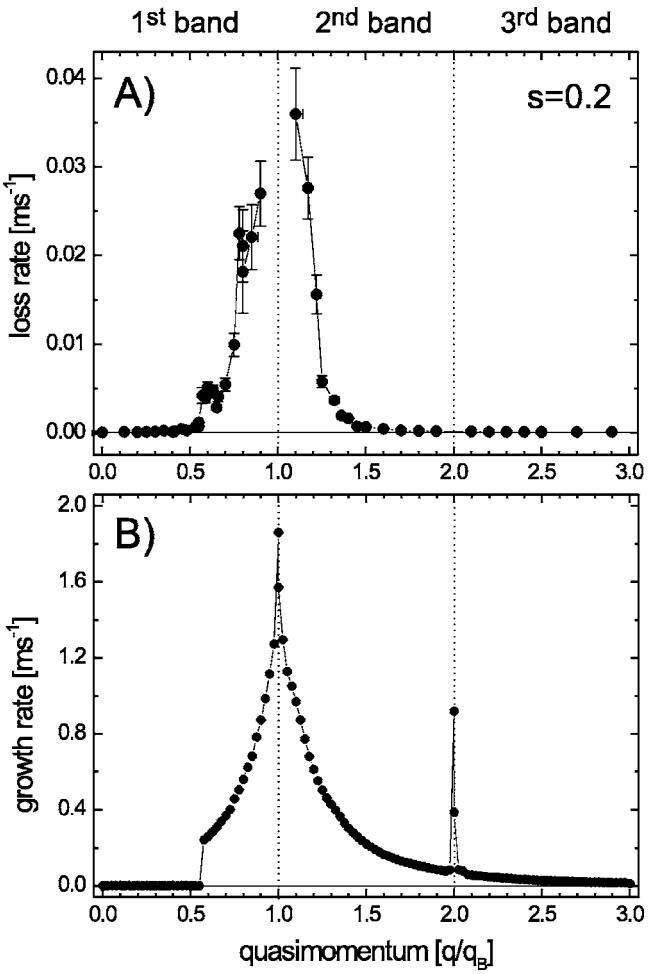

FIG. 22. Signatures of dynamical instability of a Bose condensate in an optical lattice. (a) The loss rates from a condensate held at a fixed quasimomentum q of a lattice with $s=1.15$. (b) The theoretically calculated growth rates for the dynamically most unstable mode are plotted as a function of q. Taken from Fallani *et al.*, 2004.

determining the kind of instability involved. In an early experiment by Burger *et al.* (2001), the observed breakdown of superfluidity of the condensate was initially ascribed to an energetic (Landau) instability, i.e., to the lowering of the energy of the condensate through phonon emission. Although a theoretical analysis in this direction gave plausible results, a recent calculation by Modugno *et al.* (2004) suggested that, as pointed out earlier by Burger *et al.* (2002) and Wu and Niu (2002), the onset of instability occurs well beyond the critical velocity for an energetic instability but is, in fact, consistent with a dynamic instability.

3. Dispersion management and solitons

a. Dispersion and effective mass

A matter wave inside a periodic potential exhibits a radically different response to an external force compared to the same matter wave in free space. One of the consequences of this behavior is the occurrence of Bloch oscillations as described in Sec. VI.D.1. An intuitive way

[17]In a recent experiment, Chin *et al.* (2003) investigated a single unstable mode in a condensate with attractive interactions but not confined by an optical lattice.

[18]A similar period doubling has recently been observed by Gemelke *et al.* (2005).

of taking into account the effect of the lattice on the dynamics is the introduction of the quasimomentum-dependent effective mass $m_{\mathrm{eff}}(q_0)=\hbar^2[\partial^2 E(q)/\partial q^2|_{q_0}]^{-1}$ (see Sec. IV.B.1). The dynamics of the matter wave can then be easily explained in terms of m_{eff}, whose value can be positive, negative, or zero and describes the dispersion of a wave packet.

Quantum mechanically, any wave packet with a finite width Δx will undergo dispersion in free space, i.e., it will expand with a velocity that is inversely proportional to its original size. In the presence of a periodic potential, dispersion still takes place, but now the effect of the periodicity of the potential acting on the matter wave has to be taken into account through the effective mass. As the latter can be positive or negative, the resulting dispersion can be either normal (i.e., the wave packet expands) or anomalous (i.e., the wave packet contracts). In Eiermann *et al.* (2003), Fallani *et al.* (2003), and Anker *et al.* (2004) experimentally both regimes were explored and show that an optical lattice can be used to effectively control the dispersion of a Bose-Einstein condensate. Such a dispersion management is analogous to similar schemes used in fiber optics.

The concept of effective mass can also be applied to collective excitations of the condensate. In Krämer *et al.* (2002), the modification of the frequencies of the dipole and quadrupole oscillations modes is calculated. The former corresponds to the condensate performing center-of-mass oscillations inside a harmonic trap, whereas the latter is a "breathing" oscillation. When a periodic potential is present, the frequencies of these modes are modified by a factor $\sqrt{m/m_{\mathrm{eff}}}$ and, therefore, depend on the depth of the optical lattice. This dependence was verified experimentally by Fort *et al.* (2003).

b. Solitons

When the mean-field interaction in the condensate is appreciable, new phenomena appear. If the atom-atom interaction is repulsive, it is possible to choose a *negative* effective mass $m_{\mathrm{eff}}(q_c)$ (through the corresponding quasimomentum q_c) such that the effective *attractive* interaction term in the Gross-Pitaevskii equation leads to the formation of stable bright solitons if the number of atoms is sufficiently small (see Fig. 23). These so-called gap solitons were recently observed by Eiermann *et al.* (2004).

E. Experiments in deep lattices

In the experiments discussed so far, we considered the condensate wave function to be spread out over the entire lattice. The presence of the periodic potential was taken into account through the band structure, and interaction effects were discussed within this framework. As we saw in the theoretical discussion of Sec. III, such a picture is valid when the tunneling rate between adjacent lattice sites is large compared to the band gap. If this is no longer true, it is more intuitive to look at the condensate inside the lattice as an array of localized wave functions coupled to each other through tunneling between the wells.

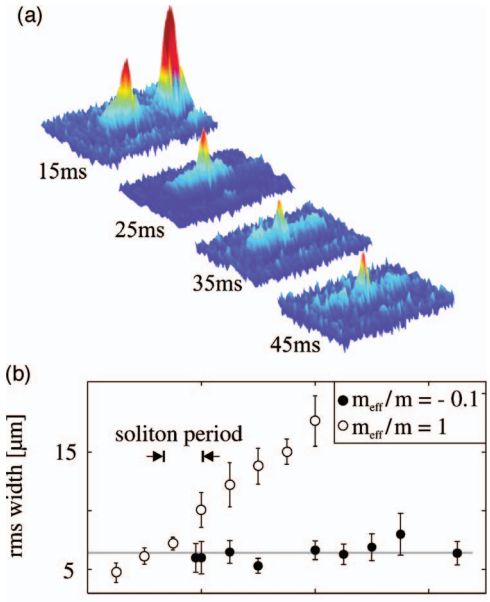

FIG. 23. (Color) Experimental demonstration of gap solitons (bright solitons for repulsive interaction in an optical lattice). (a) Absorption images revealing the *in situ* density distribution in a one-dimensional wave guide for different evolution times. Clearly, a nonspreading wave packet is formed after 25 ms. (b) The systematic measurement of the widths of the wave packets in the negative and positive mass regimes. While in the *negative mass regime* a soliton is formed whose width is constant, in the *normal mass regime* the initial atom distribution spreads out as expected. Adapted from Eiermann *et al.*, 2004.

1. Chemical potential of a BEC in an optical lattice

If the depth of the optical lattice is increased further, i.e., well above a few E_R, tunneling between the wells will quickly become negligible on the time scale of the experiments (usually a few milliseconds) as it depends exponentially on the lattice depth. At the same time, the wave functions at the individual lattice sites will be more tightly confined, resulting in an increased density. For this scenario, Pedri *et al.* (2001) calculated the "local" chemical potential of a condensate in an optical lattice with additional harmonic confinement. By letting a condensate expand freely inside a 1D lattice after switching off the initial harmonic confinement, Morsch *et al.* (2002) confirmed these calculations.

2. Josephson physics in optical lattices

Isolated condensates in the wells of a deep optical lattice can be viewed as an array of Josephson junctions. It is then useful to discretize the Gross-Pitaevskii equation (see Sec. V.B.2) and introduce a discrete nonlinear Schrödinger equation consisting of a set of coupled differential equations related to sets of neighboring lattice sites. One can further introduce "macroscopic" variables that describe the experimentally observable envelope of

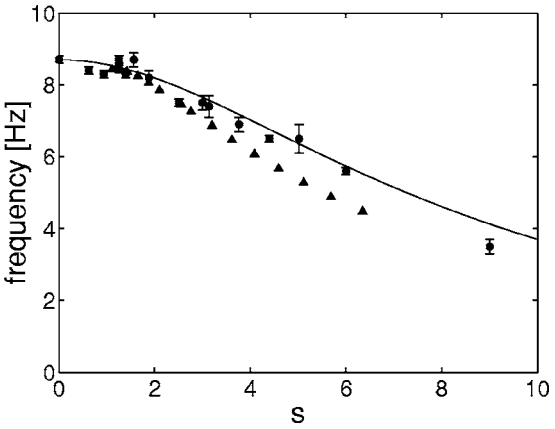

FIG. 24. Variation of the sloshing frequency of a condensate in the presence of an optical lattice of depth s. The circles are experimental data points from Cataliotti *et al.* (2001), the triangles represent the theoretical prediction based on a Josephson model (discrete nonlinear Schrödinger equation), and the solid line is a calculation based on an effective-mass approach. Taken from Krämer *et al.*, 2002.

the individual local BECs (which, in most experiments, cannot be resolved). Using this approach, Cataliotti *et al.* (2001, 2003a, 2003b) observed the motion of this envelope when the harmonic trap superposed onto the optical lattice was suddenly displaced, leading to an overall sloshing motion of the envelope and, locally, to coherent tunneling between the lattice wells and an associated "Josephson current." The dependence of the sloshing frequency on the lattice depth (see Fig. 24), which was varied between $s \approx 1$ and $s \approx 9$, indirectly reflected the critical Josephson current I_c. Alternatively, it is possible to go back to a continuum description and explain the variation in sloshing frequency in terms of the effective mass (see Sec. IV.B.1). Using this approach, Krämer *et al.* (2002) accurately reproduced (see Fig. 24) the experimental data of Cataliotti *et al.* (2001) and thereby established a link between the effective-mass regime and the Josephson interpretation of Cataliotti *et al.* (2001).

As expected, when this current exceeded a critical value, the coherent oscillations broke down and the envelope was smeared out.

3. Number squeezing and the Mott-insulator transition

Increasing the lattice depth and thus reducing the tunneling rate between adjacent wells can also be viewed as a reduction of the number fluctuations at each lattice site. As it becomes less likely for the atoms to hop between wells, the number variance σ_n goes down. Quantum mechanically, this implies that the phase variance σ_ϕ, describing the spread in relative phases between the lattice wells, has to increase. This follows from an uncertainty principle involving the product $\sigma_n \sigma_\phi$, and its effects can be seen directly by looking at the interference pattern of a BEC released from an optical lattice. In the first experiment performed by Orzel *et al.* (2001), the authors adiabatically loaded condensates of Rb atoms into deep 1D optical lattices and characterized the quality of the interference pattern through the width of the interference peaks (see Sec. VI.A) after a time of flight (see Fig. 25). As the ratio of the mean-field energy per particle to the tunneling energy decreased when the lattice depth was increased, the interference pattern was increasingly washed out. This alone proves only that phase coherence between adjacent wells was lost, but not *how* it was lost (see, for comparison, Sec. VI.C). In order to show that the loss of coherence was actually due to suppressed number fluctuations and hence the creation of number-squeezed states, the authors adiabatically lowered the lattice depth again and found that, indeed, phase coherence was restored.[19]

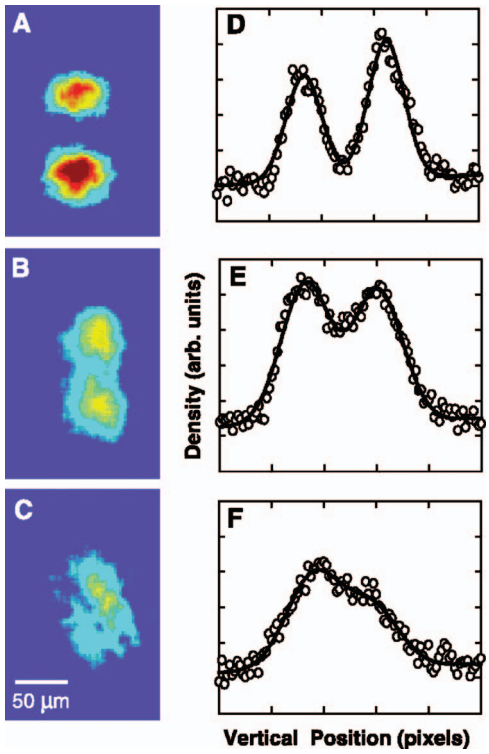

FIG. 25. (Color) Interference pictures and integrated profiles for small (a,d), intermediate (b,e), and large (c,f) lattice depths in the experiment of Orzel *et al.* (2001). As the lattice depths increase, the interference patterns become more and more "smeared out."

In a similar experiment, but using a 3D optical lattice, Greiner *et al.* (2002a) took this approach one step further and reached the Mott-insulator transition (see Sec. V.G). In this quantum phase transition, the number fluctuations actually vanish and the system reaches a state in which all the lattice wells are occupied by a well-defined number of atoms. As in the experiment by Orzel *et al.*

[19]We note here that the experiment by Orzel *et al.* (2001) has been the subject of considerable debate within the community, the consensus being that its findings are somewhat difficult to interpret [see, e.g., Pitaevskii and Stringari (2001)]. Also, one has to keep in mind that in some cases interference patterns can appear when intuitively one would not expect to see them, e.g., in the experiment of Hadzibabic *et al.* (2004).

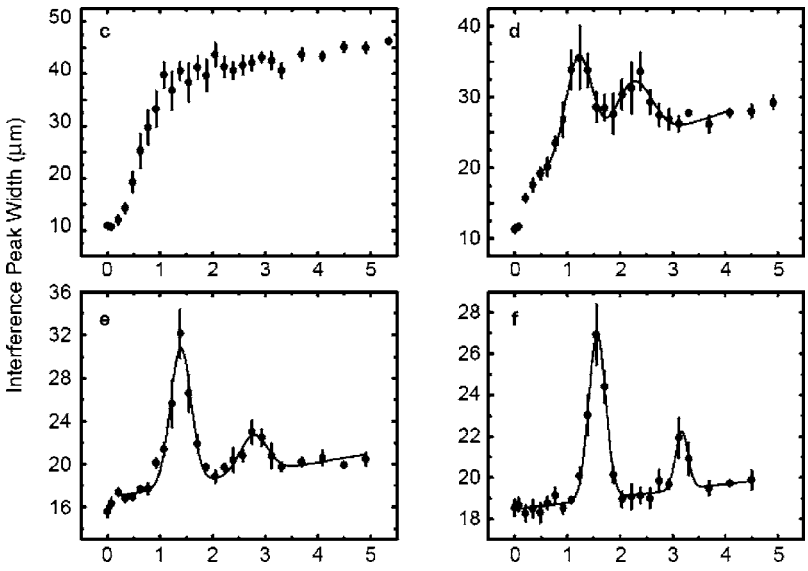

FIG. 26. The excitation spectrum of a superfluid (c) and a Mott insulator state (d)–(f) measured by applying an energy gradient between adjacent wells in the experiment of Greiner *et al.* (2002a). From (c) to (f), the lattice depth is increased, and the discrete excitation spectrum of the Mott insulator becomes visible. The horizontal axes indicate the potential gradient expressed in kHz.

(2001), the telltale sign for the increasing phase fluctuations that go hand in hand with the decreasing number fluctuations as the lattice depth is increased was the deterioration of the interference pattern. Again, this observation on its own does not unambiguously demonstrate the transition from the initial superfluid to a Mott-insulator state (Roth and Burnett, 2003). A further piece of evidence in the experiment by Greiner *et al.* (2002a) was the occurrence of a gap in the excitation spectrum of the Mott insulator (see Fig. 26). By applying a magnetic field gradient to the lattice (which amounts to "tilting" it), an energy difference between adjacent sites was created that allowed atoms to hop between the sites. Whereas in the superfluid regime (for small lattice depths) this hopping increases continuously with the energy difference between the sites, in the Mott-insulator regime only well-defined energy differences are allowed, corresponding to the energy "penalty" for adding an atom to a lattice site already occupied by an atom (or several atoms). In their experiment, the authors also demonstrated that the Mott insulator transition is reversible by lowering the optical lattice depth. Similar results were obtained by Stöferle *et al.* (2004) and Köhl *et al.* (2005) using lattices in one, two, and three dimensions (see Sec. VII).

F. Optical lattices as a tool

In the experiments described thus far, the main interest lay in the properties of the system BEC plus optical lattices that are intimately linked to the periodicity of the lattice and hence to the band structure or, in the deep lattice limit, to the periodic array of local wave functions. An optical lattice can, however, also be used as a tool to create, for instance, multiple condensates with different momenta from a single one by Bragg diffraction, or to probe coherence properties of a BEC in particular regimes where interesting physics happens that is not associated with the presence of the lattice. In this section, we shall briefly describe some of the experiments falling into this category.

1. Creating momentum components with an optical lattice

When an optical lattice moving at a velocity $v=v_R$ is switched on suddenly, the condensate wave function is projected onto the lowest two energy bands (see Sec. VI.B). When the lattice is switched off abruptly, the plane waves corresponding to the bands at the edge of the Brillouin zone interfere with the phases they accumulated while the lattice was on, splitting the condensate into two momentum components with weights depending on the length of the interaction and the lattice depth (Kozuma *et al.*, 1999). Alternatively, this process can be viewed as first-order Bragg diffraction.

Using this technique, Deng *et al.* (1999b) split up a condensate into three momentum components by applying two sequences of Bragg pulses with the lattice. Whereas in a linear approximation these momentum components would fly apart independently, the nonlinear interaction between them led to the creation of a fourth wave packet having a momentum that fulfilled the condition for four-wave mixing, a process well known from nonlinear optics.

Splitting the condensate into several momentum components can also be used for the realization of matter-wave interferometry with BECs. By splitting the condensate in two and recombining the fragments after a variable time, Simsarian *et al.* (2000) observed the phase evolution of a condensate after it had been released from a magnetic trap. Various other experiments involving several momentum components of condensates have been carried out, ranging from coherence measurements to a matter-wave realization of the Talbot effect (Deng *et al.*, 1999a; Hagley *et al.*, 1999; Ovchinnikov *et al.*, 1999).

2. Measuring the excitation spectrum of a condensate

The Bragg pulses described above can generally be used to excite phonons and to transfer momentum to the condensate (Stamper-Kurn *et al.*, 1999). In an early experiment, Stenger *et al.* (1999) determined the momentum width of a sodium BEC by measuring, effectively, the dynamic structure factor $S(\mathbf{q},\nu)$ of the condensate through the momentum transfer of the Bragg-scattered lattice photons as a function of the detuning between the two beams. Using a similar technique, Vogels *et al.* (2002) directly observed the Bogoliubov quasiparticle transformation of a condensate. Further experiments using tomographic techniques to determine the momentum transfer to the condensate were carried out by Ozeri *et al.* (2002, 2003) and Steinhauer *et al.* (2002, 2003).

3. Probing the coherence properties of a condensate

The sensitivity of Bragg diffraction to the momentum distribution can also be exploited to detect phase fluctuations in a condensate. Gerbier *et al.* (2003) and Richard *et al.* (2003) measured the Bragg diffraction efficiency as a function of detuning in the case of an extremely elongated cigar-shaped condensate (aspect ratio $\approx$150) whose 1D character led to increased phase fluctuations. These phase fluctuations were reflected in a Lorentzian-like (as opposed to Gaussian) profile of the Bragg spectrum from the width of which Richard *et al.* (2003) were able to extract the decay length L_Φ of the spatial correlation function.

4. Studying the time evolution of coherent states

Under suitable conditions, a deep optical lattice can be used to create a large number of identical copies of quantum states. For instance, below the critical depth for the Mott-insulator transition (see Sec. V.G) the matter-wave field inside a potential well of the lattice can be described to a good approximation by a coherent state, i.e., a superposition of different number states $|n\rangle$. Interactions cause these number states to evolve with different phases, leading to a loss of contrast of the interference pattern in a time-of-flight experiment after switching off the lattice. Greiner *et al.* (2002b) exploited this fact in order to map out the time evolution of the coherent states of atoms in a 3D optical lattice.

VII. CURRENT TRENDS AND FUTURE DIRECTIONS

A review paper on an active and fast-growing field such as the one discussed in the present article can, at best, provide an introduction to the general area of research and a snapshot image of the current state of the art. At the time of writing this review, many new avenues for future research on BECs in optical lattices—both theoretically and experimentally—are opening up, ranging from highly correlated systems to applications in quantum computing, where neutral atoms inside optical lattices are seen as promising candidates for quantum bits (or "qubits"). Furthermore, the general field of ultracold atoms is moving toward new goals, involving degenerate Fermi gases and molecular condensates. It is very likely that these new systems, too, will soon be combined with optical lattices (and, to some extent, they already have been, as we shall see in the following). We have no doubt that many interesting phenomena will be discovered and studied in such systems, and at this point we can only give the reader a vague idea of what we believe are promising directions to pursue.

A. 2D and 1D systems

One of the salient features of optical lattices is the large harmonic trapping frequency in the direction of the lattice. Owing to the small length scale of the interference pattern created by the lattice lasers, trapping frequencies of several tens of kHz in the potential wells of the lattice can be achieved with modest laser intensities. Comparing these to typical magnetic trapping frequencies of hundreds of Hz and to the chemical potentials of roughly the same order of magnitude usually encountered in BEC experiments, one finds that it should be possible to realize 2D (Burger *et al.*, 2002; Stock *et al.*, 2005) or 1D quantum systems by "freezing out" one or two degrees of freedom by adding a 1D or 2D optical lattice to the magnetic trap. The condition for a condensate to exhibit 2D or 1D characteristics is that the healing length $\xi=\sqrt{4\pi na}$ be smaller than one or two of the harmonic-oscillator lengths $l_i=(\hbar/m\omega_i)^{1/2}$ associated with the trapping frequencies ω_i, respectively. Here, n is the density and a the s-wave scattering length, as usual. The crossover to the 2D and 1D regimes was achieved by Görlitz *et al.* (2001) using dipole traps and lowering the number of atoms in order to satisfy the above conditions. Exploiting the large trapping frequencies of optical lattices, Moritz *et al.* (2003) and Stöferle *et al.* (2004) created 2D and 1D condensates by loading an "ordinary" BEC from a magnetic trap into a configuration of three perpendicular lattice beams. One or two of the lattices were then made very deep (tens of E_R), resulting in a stack of pancake-shaped 2D condensates or a grid of cigar-shaped 1D condensates ("tubes") (see Fig. 27). With this method, the authors were able to enter the *strongly interacting* regime for a 1D gas which, counterintuitively, is reached for *small* atomic densities inside the 1D tubes. In their experiments, each of the tubes contained only a few dozen atoms. Whereas in a single dipole trap such a small atom number would hardly be observable, in an array of 1D tubes created by a 2D lattice the experiment is effectively carried out in parallel in hundreds of tubes, leading to an easily detectable signal. For the 1D case, Stöferle *et al.* (2004) observed a lowering of the critical parameter $(U/J)_c$ (see Sec. V.G) due to increased quantum fluctuations, as expected from theory. The role of these fluctuations and the resulting reduction of the three-body correlation function were also investigated by Laburthe Tolra *et al.* (2004) through the measurement of a reduced three-body recombination rate.

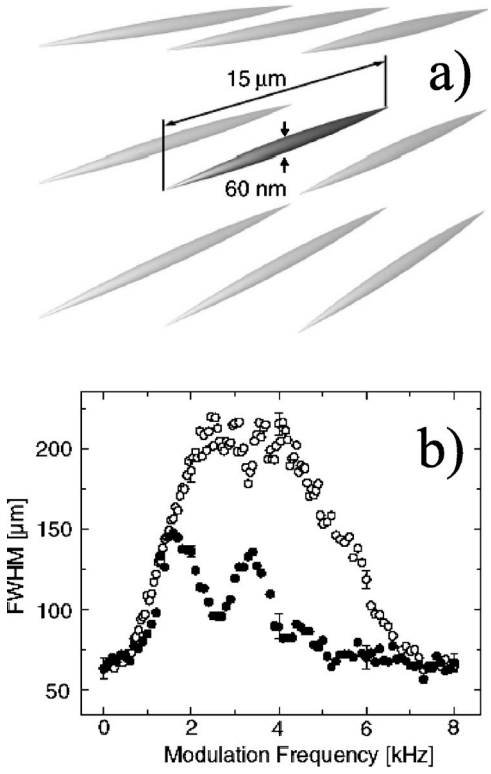

FIG. 27. (a) An array of "tubes" created by a two-dimensional optical lattice, as used in the experiment of Stöferle *et al.* (2004) to realize the Mott-insulator transition in one dimension, and (b) the excitation spectrum of the 1D Mott insulator. The spacing between adjacent tubes in (a) is 413 nm. Taken from Moritz *et al.*, 2003 and Stöferle *et al.*, 2004.

In a similar experiment, Paredes *et al.* (2004) realized the Tonks regime in which the repulsive interactions between the atoms completely dominate the physics. The system then behaves like a fermionic gas, i.e., two particles are never found in the same position, although the atoms are actually bosons. In this experiment, the effective mass of the atoms is increased through the optical lattice along the direction of the tubes so that the Tonks regime can be more easily reached. Kinoshita *et al.* (2004) also reached the Tonks-Girardeau regime using a two-dimensional optical lattice in order to create a one-dimensional quantum gas.

B. Fermions in lattices

In the early 1990s, experimental studies on ultracold bosonic atoms were largely driven by the quest for obtaining Bose-Einstein condensation. Research on BECs is still a thriving field, but more recently fermions have also caused a lot of excitement in atomic physics. Obviously, in the case of fermions the principal interest lies in the fact that electrons in solid-state crystals are fermions. Ultracold, dilute clouds of fermionic atoms hence offer the enticing prospect of studying phenomena like the BCS transition to superconductivity in a model system whose parameters can easily be controlled. Adding a periodic potential is, therefore, a natural further step in that direction. So far, fermions in an optical lattice have been studied experimentally by Modugno *et al.* (2003) using ^{40}K atoms in a one-dimensional lattice. After cooling the atoms down to a third of the Fermi temperature T_F=430 nK, they switched on an optical lattice with s=8. The fermionic character of ^{40}K was clearly seen by comparing sloshing oscillations between bosons and fermions in the superimposed magnetic trap while the lattice was present. Since the initial quasimomentum distribution of the fermions was much larger than that of the bosons due to the exclusion principle, the sloshing motion of the fermions was heavily damped in contrast to the undamped oscillations of the bosons. In a proof-of-principle experiment, Roati *et al.* (2004) have also shown that fermions should be ideally suited to precision measurements in optical lattices, e.g., for a determination of the Earth's acceleration through the frequency of Bloch oscillations, because in contrast to bosons they do not interact with each other, eliminating dephasing effects due to the mean-field interaction in a BEC.

On the theoretical side, Ruostekoski and Javanainen (Ruostekoski *et al.*, 2002; Javanainen and Ruostekoski, 2003) have investigated the possibility of observing a fractional fermion particle number inside an optical lattice. Such an effect is predicted to occur in the presence of a topologically nontrivial bosonic background field and is related, e.g., to the fractional quantum Hall effect.

C. Mixtures

Up to now, experiments with BECs in optical lattices have been almost exclusively done with a single atomic species in a single spin state. Recently, a number of theoretical studies have been published in which a host of new phenomena are predicted if more than one spin state or atomic species is used, especially if one of the species is bosonic and the other fermionic.

A mixture of bosonic and fermionic atoms in an optical lattice produces extremely rich physics. Studying these mixtures in different regimes, Lewenstein *et al.* (2004) found several new quantum phases containing composite fermions (made up from a fermion and one or several bosons) which could be either delocalized superfluid or metallic phases or localized density wave or domain insulator phases. Similar studies have been done by several other authors (Albus *et al.*, 2003; Büchler and Blatter, 2003; Roth and Burnett, 2004).

Another interesting aspect of a boson-fermion mixture is the possibility to create an array of dipolar molecules. Moore and Sadeghpour (2003) show that this can be achieved by first creating a combined Mott insulator state with one atom of both species per lattice site and then creating molecules by photoassociation. The dipolar molecules thus created could either be used as a resource for quantum computing (see Sec. VII.E) or be transformed into a dipolar condensate by melting the Mott-insulator phase.

In a first experiment combining bosons and fermions in a lattice, Ott *et al.* (2004) have investigated the effect of a bosonic bath on fermions moving through an optical

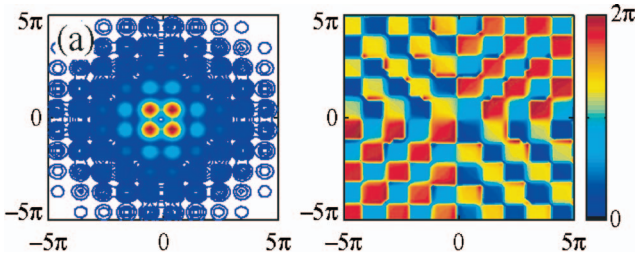

FIG. 28. (Color) Density (left) and phase profile (right) of a gap vortex in a two-dimensional optical lattice. The x and y axes are labeled in units of d/π, where d is the lattice spacing. Taken from Ostrovskaya and Kivshar, 2004a.

lattice. The results of these experiments show that, just as in condensed matter physics, interactions lead to a fermionic current that would be absent if the fermions moved on their own inside the periodic potential.

D. Vortices in lattices

Vortices in Bose-Einstein condensates are an intriguing quantum phenomenon directly linked to the superfluidity of this system and have been studied extensively both experimentally and theoretically (Madison *et al.*, 2000; McGee and Holland, 2001). Recently, a number of theoretical papers have dealt with systems combining vortices and optical lattices. Intuitively, a single vortex and a one-dimensional lattice can be combined by applying the lattice either *along* the direction of the vortex or *perpendicular* to it. The former case was studied by Martikainen and Stoof (2003b, 2004) and is particularly interesting because of its analogies with high-T_c superconductivity and the possibility of realizing the quantum Hall regime for BECs in a lattice. The case of a vortex perpendicular to the lattice direction was discussed by Kevrekidis *et al.* (2003) and Bhattacherjee *et al.* (2004).

Exploiting an analogy with the gap solitons discussed in Sec. V.B.1, Ostrovskaya and Kivshar (2004a) have recently investigated the possibility of creating "gap vortices" in optical lattices (see Fig. 28). They also address the general problem of the localization of topological defects in deep lattices.

E. Quantum computing

The idea of building a quantum computer has motivated both theoretical and experimental efforts for more than a decade. Originally conceived by Richard Feynman as a "quantum simulator" capable of calculating the dynamics of complex quantum systems, it has since become the paradigm for a new generation of computers that could solve problems out of the reach of classical computers, such as the factorization of large numbers.[20]

A first step in this direction was made by Greiner *et al.* (2002a) in their demonstration of the Mott-insulator transition (see Sec. VI.E.3), in which a state with exactly one atom per lattice site is created starting from a BEC. In a subsequent experiment, the authors also showed that in such a system controlled collisions between atoms in two overlapping optical lattices can be used to create entanglement (Bloch *et al.*, 2003; Mandel *et al.*, 2003a, 2003b), which besides the superposition principle is the second essential resource of quantum computing.

Neutral atoms in optical lattices have a number of attractive features that make them interesting candidates for the realization of a quantum computer (Deutsch *et al.*, 2000; Porto *et al.*, 2003; Jaksch, 2004). One of them is their intrinsic scalability, i.e., the fact that it is, in principle, not difficult to realize 1D, 2D, or 3D arrays of individually trapped atoms with large numbers of sites. Among other things, this should make possible the creation of so-called "cluster states" which represent a one-way quantum computer capable of carrying out a quantum computation with a single read-out (Raussendorf and Briegel, 2001; Raussendorf *et al.*, 2003).

VIII. CONCLUSIONS

Bose-Einstein condensates in optical lattices constitute an active field of research that has already spawned several different subfields. Roughly speaking, the current experimental and theoretical efforts can be divided into three categories: nonlinear matter waves, strongly correlated many-particle systems, and quantum computation. In the latter, optical lattices are used mainly as a tool for preparing and "engineering" quantum states in a controlled way so that they can then be used for the implementation of quantum algorithms. In the first two categories, the full control over the system's parameters is exploited in several ways. By changing the geometry of the lattice and combining, e.g., different atomic species, one can realize many-body Hamiltonians that are not easily accessible in condensed matter systems and hence use BECs in lattices as a model system in order to test theoretical predictions. Likewise, in the physics of nonlinear matter waves, the control over the lattice geometry gives BECs in periodic structures an edge over similar realizations in nonlinear optics. Whereas the latter are limited to two dimensions, BECs in lattices can be used to study nonlinear dynamics of three-dimensional systems.

Although it is difficult to predict which of these three directions will play the most important role in the future development of the field, it is likely that all of them will lead to interesting new results. This will also depend to a large extent on the fruitful interactions between different communities. Just as the possibility of studying the Bose-Hubbard model in optical lattices has sparked the interest of the condensed matter community, the links between nonlinear optics and nonlinear matter waves in periodic potentials have started to attract a number of researchers from the former community to interact with the Bose-Einstein condensation community. And who

[20]A good overview of the state of the art of the field and prospects for the future can be found in the QIST Quantum Computing Roadmap (http://qist.lanl.gov/).

knows, many more as yet unexplored avenues might open up that, right now, no one is even thinking about.

ACKNOWLEDGMENTS

We thank Ennio Arimondo, Chiara Fort, Mattia Jona-Lasinio, Klaus Mølmer, and Jörg Helge Müller for a careful reading of the manuscript and many helpful suggestions. We further wish to acknowledge the European Union RTN-Network "Cold Quantum Gases" Contract No. HPRN-CT-2000-00125 for making visits possible by providing travel money. M.O. acknowledges the financial support of the Deutsche Forschungsgemeinschaft (Emmy Noether Program).

REFERENCES

Abdullaev, F. K., B. B. Baizakov, S. A. Darmanyan, V. V. Konotop, and M. Salerno, 2001, Phys. Rev. A **64**, 043606.
Abdullaev, F. K., B. B. Baizakov, and M. Salerno, 2003, Phys. Rev. E **68**, 066605.
Agrawal, G., 2001, *Applications of Nonlinear Fiber Optics*, 2nd ed. (Academic, San Diego).
Ahufinger, V., and A. Sanpera, 2005, Phys. Rev. Lett. **94**, 130403.
Ahufinger, V., A. Sanpera, P. Pedri, L. Santos, and M. Lewenstein, 2004, Phys. Rev. A **69**, 053604.
Albus, A., F. Illuminati, and J. Eisert, 2003, Phys. Rev. A **68**, 023606.
Alfimov, G. L., P. G. Kevrekidis, V. V. Konotop, and M. Salerno, 2002a, Phys. Rev. E **66**, 046608.
Alfimov, G. L., V. V. Konotop, and M. Salerno, 2002b, Europhys. Lett. **58**, 7.
Anderson, B. P., and M. A. Kasevich, 1998, Science **282**, 1686.
Anglin, J. R., 2003, Phys. Rev. A **67**, 051601(R).
Anker, T., M. Albiez, B. Eiermann, M. Taglieber, and M. K. Oberthaler, 2004, Opt. Express **12**, 11.
Anker, T., M. Albiez, R. Gati, S. Hunsmann, B. Eiermann, A. Trombettoni, and M. K. Oberthaler, 2005, Phys. Rev. Lett. **94**, 020403.
Ashcroft, N. J., and N. D. Mermin, 1976, *Solid State Physics* (International Thomson Publishing, New York).
Baizakov, B. B., V. V. Konotop, and M. Salerno, 2002, J. Phys. B **35**, 5105.
Barone, A., 2000, *Quantum Mesoscopic Phenomena and Mesoscopic Devices in Microelectronics* (Kluwer Academic, Dordrecht, The Netherlands).
Baym, G., and C. J. Pethick, 1996, Phys. Rev. Lett. **76**, 6.
Bender, C., and S. Orszag, 1978, *Advanced Mathematical Methods for Scientists and Engineers: Asymptotic Methods and Perturbation Theory* (Springer, New York).
Berg-Sørensen, K., and K. Mølmer, 1998, Phys. Rev. A **58**, 1480.
Bhattacherjee, A. B., O. Morsch, and E. Arimondo, 2004, J. Phys. B **37**, 2355.
Bloch, I., 2004, Phys. World **April**, 25.
Bloch, I., 2005, J. Phys. B **38**, S629.
Bloch, I., M. Greiner, O. Mandel, and T. W. Hänsch, 2003, Proc. R. Soc. London, Ser. A **361**, 1409.
Bogoliubov, N., 1947, J. Phys. (Moscow) **11**, 23.
Brazhnyi, V. A., and V. V. Konotop, 2004, Mod. Phys. Lett. B **18**, 627.
Bronski, J. C., L. D. Carr, B. Deconinck, and J. N. Kutz, 2001a, Phys. Rev. Lett. **86**, 1402.
Bronski, J. C., L. D. Carr, B. Deconinck, J. N. Kutz, and K. Promislow, 2001b, Phys. Rev. E **63**, 036612.
Buchleitner, A., and A. R. Kolovsky, 2003, Phys. Rev. Lett. **91**, 253002.
Büchler, H. P., and G. Blatter, 2003, Phys. Rev. Lett. **91**, 130404.
Burger, S., F. S. Cataliotti, C. Fort, P. Maddaloni, F. Minardi, and M. Inguscio, 2002, Europhys. Lett. **57**, 1.
Burger, S., F. S. Cataliotti, C. Fort, F. Minardi, M. Inguscio, M. L. Chiofalo, and M. P. Tosi, 2001, Phys. Rev. Lett. **86**, 4447.
Burger, S., F. S. Cataliotti, C. Fort, F. Minardi, M. Ignuscio, M. L. Chiofalo, and M. P. Tosi, 2002, Phys. Rev. Lett. **89**, 088902.
Cataliotti, F. S., S. Burger, C. Fort, P. Maddaloni, F. Minardi, A. Trombettoni, A. Smerzi, and M. Inguscio, 2001, Science **293**, 843.
Cataliotti, F. S., L. Fallani, F. Ferlaino, C. Fort, P. Maddaloni, and M. Inguscio, 2003a, J. Opt. B: Quantum Semiclassical Opt. **5**, S17.
Cataliotti, F. S., L. Fallani, F. Ferlaino, C. Fort, P. Maddaloni, and M. Inguscio, 2003b, New J. Phys. **5**, 71.
Chin, J. K., J. M. Vogels, and W. Ketterle, 2003, Phys. Rev. Lett. **90**, 160405.
Chiofalo, M. L., M. Polini, and M. P. Tosi, 2000, Eur. Phys. J. D **11**, 371.
Chiofalo, M. L., and M. P. Tosi, 2000, Phys. Lett. A **268**, 406.
Chiofalo, M. L., and M. P. Tosi, 2001, J. Phys. B **34**, 4551.
Choi, D.-I., and Q. Niu, 1999, Phys. Rev. Lett. **82**, 2022.
Christodoulides, D. N., F. Lederer, and Y. Silberberg, 2003, Nature (London) **424**, 817.
Chu, S., 1998, Rev. Mod. Phys. **70**, 685.
Cohen-Tannoudji, C., 1998, Rev. Mod. Phys. **70**, 707.
Cornell, E. A., and C. E. Wieman, 2002, Rev. Mod. Phys. **74**, 875.
Cristiani, M., O. Morsch, N. Malossi, M. Jona-Lasinio, M. Anderlini, E. Courtade, and E. Arimondo, 2004, Opt. Express **12**, 4.
Cristiani, M., O. Morsch, J. H. Müller, D. Ciampini, and E. Arimondo, 2002, Phys. Rev. A **65**, 063612.
Dahan, M. B., E. Peik, J. Reichel, Y. Castin, and C. Salomon, 1996, Phys. Rev. Lett. **76**, 4508.
Dalfovo, F., S. Giorgini, L. P. Pitaevskii, and S. Stringari, 1999, Rev. Mod. Phys. **71**, 463.
Dauxois, T., and M. Peyrard, 1993, Phys. Rev. Lett. **70**, 3935.
Dauxois, T., S. Ruffo, and A. Torcini, 1997, Phys. Rev. E **56**, R6229.
Deng, L., E. W. Hagley, J. Denschlag, J. E. Simsarian, M. Edwards, C. W. Clark, K. Helmerson, S. L. Rolston, and W. D. Phillips, 1999a, Phys. Rev. Lett. **83**, 5407.
Deng, L., E. W. Hagley, J. Wen, M. Trippenbach, Y. Band, P. S. Julienne, J. E. Simsarian, K. Helmerson, S. L. Rolston, and W. D. Phillips, 1999b, Nature (London) **398**, 218.
Denschlag, J. H., J. E. Simsarian, H. Häffner, C. McKenzie, A. Browaeys, D. Cho, K. Helmerson, S. L. Rolston, and W. D. Phillips, 2002, J. Phys. B **35**, 3095.
deSterke, C. M., and J. E. Sipe, 1994, in *Progress in Optics*, edited by E. Wolf (North-Holland, Amsterdam), Vol. XXXIII, p. 203.
Deutsch, I. H., G. K. Brennen, and P. S. Jessen, 2000, Fortschr. Phys. **48** (9-11), 925.
Diakonov, D., L. M. Jensen, C. J. Pethick, and H. Smith, 2002, Phys. Rev. A **66**, 013604.

Efremidis, N. K., J. Hudock, D. N. Christodoulides, J. W. Fleischer, O. Cohen, and M. Segev, 2003, Phys. Rev. Lett. **91**, 213906.
Eggleton, B. J., R. E. Slusher, C. M. deSterke, P. A. Krug, and J. E. Sipe, 1996, Phys. Rev. Lett. **76**, 1627.
Eiermann, B., T. Anker, M. Albiez, M. Taglieber, P. Treutlein, K.-P. Marzlin, and M. K. Oberthaler, 2004, Phys. Rev. Lett. **92**, 230401.
Eiermann, B., P. Treutlein, T. Anker, M. Albiez, M. Taglieber, K.-P. Marzlin, and M. K. Oberthaler, 2003, Phys. Rev. Lett. **91**, 060402.
Fallani, L., F. S. Cataliotti, J. Catani, C. Fort, M. Modugno, M. Zawada, and M. Inguscio, 2003, Phys. Rev. Lett. **91**, 240405.
Fallani, L., L. DeSarlo, J. E. Lye, M. Modugno, R. Saers, C. Fort, and M. Inguscio, 2004, Phys. Rev. Lett. **93**, 140406.
Fisher, M. P. A., P. B. Weichman, G. Grinstein, and D. S. Fisher, 1989, Phys. Rev. B **40**, 546.
Fort, C., F. S. Cataliotti, L. Fallani, F. Ferlaino, P. Maddaloni, and M. Inguscio, 2003, Phys. Rev. Lett. **90**, 140405.
Friebel, S., C. DÁndrea, J. Walz, M. Weitz, and T. W. Hänsch, 1998, Phys. Rev. A **57**, R20.
Gemelke, N., E. Sarajlic, Y. Bidel, S. Hong, and S. Chu, 2005, e-print cond-mat/0504311.
Gerbier, F., J. H. Thywissen, S. Richard, M. Hugbart, P. Bouyer, and A. Aspect, 2003, Phys. Rev. A **67**, 051602(R).
Giltner, D. M., R. W. McGowan, and S. A. Lee, 1995, Phys. Rev. A **52**, 3966.
Görlitz, A., J. M. Vogels, A. E. Leanhardt, C. Raman, T. L. Gustavson, J. R. Abo-Shaeer, A. P. Chikkatur, S. Gupta, S. Inouye, T. Rosenband, and W. Ketterle, 2001, Phys. Rev. Lett. **87**, 130402.
Gould, P. L., G. A. Ruff, and D. E. Pritchard, 1986, Phys. Rev. Lett. **56**, 827.
Greiner, M., I. Bloch, O. Mandel, T. W. Hänsch, and T. Esslinger, 2001a, Appl. Phys. B: Lasers Opt. **73**, 769.
Greiner, M., I. Bloch, O. Mandel, T. W. Hänsch, and T. Esslinger, 2001b, Phys. Rev. Lett. **87**, 160405.
Greiner, M., O. Mandel, T. Esslinger, T. W. Hänsch, and I. Bloch, 2002a, Nature (London) **415**, 39.
Greiner, M., O. Mandel, T. W. Hänsch, and I. Bloch, 2002b, Nature (London) **419**, 51.
Grimm, R., M. Weidemüller, and Y. B. Ovchinnikov, 2000, Adv. At., Mol., Opt. Phys. **42**, 95.
Grynberg, G., and C. Robilliard, 2001, Phys. Rep. **355**, 335.
Hadzibabic, Z., S. Stock, B. Battelier, V. Bretin, and J. Dalibard, 2004, Phys. Rev. Lett. **93**, 180403.
Hagley, E. W., L. Deng, M. Kozuma, M. Trippenbach, Y. B. Band, M. Edwards, M. Doery, P. S. Julienne, K. Helmerson, S. L. Rolston, and W. D. Phillips, 1999, Phys. Rev. Lett. **83**, 3112.
Hilligsoe, K. M., M. K. Oberthaler, and K.-P. Marzlin, 2002, Phys. Rev. A **66**, 063605.
Iliescu, D., S. Fishman, and E. Ben-Jacob, 1992, Phys. Rev. B **46**, 14675.
Jaksch, D., 2004, Contemp. Phys. **45**, 367.
Jaksch, D., H.-J. Briegel, J. I. Cirac, C. W. Gardiner, and P. Zoller, 1999, Phys. Rev. Lett. **82**, 1975.
Jaksch, D., C. Bruder, J. I. Cirac, C. W. Gardiner, and P. Zoller, 1998, Phys. Rev. Lett. **81**, 3108.
Jaksch, D., and P. Zoller, 2005, Ann. Phys. (N.Y.) **315**, 52.
Javanainen, J., 1999, Phys. Rev. A **60**, 4902.
Javanainen, J., and J. Ruostekoski, 2003, Phys. Rev. Lett. **91**, 150404.
Jessen, P. S., and I. H. Deutsch, 1996, Adv. At., Mol., Opt. Phys. **37**, 95.
Jona-Lasinio, M., O. Morsch, M. Cristiani, N. Malossi, J. H. Müller, E. Courtade, M. Anderlini, and E. Arimondo, 2003, Phys. Rev. Lett. **91**, 230406.
Kalosakas, G., K. Ø. Rasmussen, and A. R. Bishop, 2002, Phys. Rev. Lett. **89**, 030402.
Ketterle, W., 2002, Rev. Mod. Phys. **74**, 1131.
Ketterle, W., D. Durfee, and D. M. Stamper-Kurn, 1999, in *Bose-Einstein Condensation in Atomic Gases, Proceedings of the International School of Physics "Enrico Fermi," Course CXL*, edited by M. Inguscio, S. Stringari, and C. Wieman (IOS, Amsterdam), pp. 67–176.
Kevrekidis, P. G., R. Carretero-Gonzalez, G. Theocharis, D. J. Frantzeskakis, and B. A. Malomed, 2003, J. Phys. B **36**, 3467.
Kinoshita, T., T. Wenger, and D. S. Weiss, 2004, Nature (London) **305**, 1125.
Kittel, C., 1996, *Introduction to Solid State Physics* (Wiley, New York).
Köhl, M., H. Moritz, T. Stöferle, C. Schori, and T. Esslinger, 2005, J. Low Temp. Phys. **138**, 635.
Kolovsky, A. R., 2003, Phys. Rev. Lett. **90**, 213002.
Konotop, V. V., and M. Salerno, 2002, Phys. Rev. A **65**, 021602(R).
Kozuma, M., L. Deng, E. W. Hagley, J. Wen, R. Lutwak, K. Helmerson, S. L. Rolston, and W. D. Phillips, 1999, Phys. Rev. Lett. **82**, 871.
Krämer, M., C. Menotti, L. Pitaevskii, and S. Stringari, 2003, Eur. Phys. J. D **27**, 247.
Krämer, M., L. Pitaevskii, and S. Stringari, 2002, Phys. Rev. Lett. **88**, 180404.
Laburthe Tolra, B., K. M. O'Hara, J. H. Huckans, W. D. Phillips, S. L. Rolston, and J. V. Porto, 2004, Phys. Rev. Lett. **92**, 190401.
Leggett, A. J., 2001, Rev. Mod. Phys. **73**, 307.
Lenz, G., P. Meystre, and E. M. Wright, 1994, Phys. Rev. A **50**, 1681.
Letokohov, V., and V. Minogin, 1977, Phys. Lett. **61A**, 370.
Lewenstein, M., L. Santos, M. A. Baranov, and H. Fehrmann, 2004, Phys. Rev. Lett. **92**, 050401.
Liu, J., L. Fu, B.-Y. Ou, S.-G. Chen, D.-I. Choi, B. Wu, and Q. Niu, 2002, Phys. Rev. A **66**, 023404.
Louis, P. J. Y., E. A. Ostrovskaya, C. M. Savage, and Y. S. Kivshar, 2003, Phys. Rev. A **67**, 013602.
Machholm, M., A. Nicolin, C. J. Pethick, and H. Smith, 2004, Phys. Rev. A **69**, 043604.
Machholm, M., C. J. Pethick, and H. Smith, 2003, Phys. Rev. A **67**, 053613.
Madison, K. W., F. Chevy, W. Wohlleben, and J. Dalibard, 2000, Phys. Rev. Lett. **84**, 806.
Mandel, O., M. Greiner, A. Widera, T. Rom, T. W. Hänsch, and I. Bloch, 2003a, Nature (London) **425**, 937.
Mandel, O., M. Greiner, A. Widera, T. Rom, T. W. Hänsch, and I. Bloch, 2003b, Phys. Rev. Lett. **91**, 010407.
Martikainen, J.-P., and H. T. C. Stoof, 2003a, Phys. Rev. A **68**, 013610.
Martikainen, J.-P., and H. T. C. Stoof, 2003b, Phys. Rev. Lett. **91**, 240403.
Martikainen, J.-P., and H. T. C. Stoof, 2004, Phys. Rev. A **69**, 053617.
McGee, S. A., and M. J. Holland, 2001, Phys. Rev. A **63**, 043608.
Meacher, D. R., 1998, Contemp. Phys. **39**, 329.

Mellish, A. S., G. Duffy, C. McKenzie, R. Geursen, and A. C. Wilson, 2003, Phys. Rev. A **68**, 051601(R).
Menotti, C., M. Krämer, L. Pitaevskii, and S. Stringari, 2003a, Phys. Rev. A **67**, 053609.
Menotti, C., A. Smerzi, and A. Trombettoni, 2003b, New J. Phys. **5**, 112.1.
Metcalf, H. J., and P. van der Straten, 1999, *Laser Cooling and Trapping* (Springer, New York).
Modugno, G., F. Ferlaino, R. Heidemann, G. Roati, and M. Inguscio, 2003, Phys. Rev. A **68**, 011601(R).
Modugno, M., C. Tozzo, and F. Dalfovo, 2004, Phys. Rev. A **70**, 043625.
Moore, M. G., and H. R. Sadeghpour, 2003, Phys. Rev. A **67**, 041603(R).
Moritz, H., T. Stöferle, M. Köhl, and T. Esslinger, 2003, Phys. Rev. Lett. **91**, 250402.
Morsch, O., and E. Arimondo, 2002, in *Dynamics and Thermodynamics of Systems with Long-Range Interactions*, edited by T. Dauxois, S. Ruffo, E. Arimondo, and M. Wilkens (Springer-Verlag, Berlin), pp. 312–331.
Morsch, O., M. Cristiani, J. H. Müller, D. Ciampini, and E. Arimondo, 2002, Phys. Rev. A **66**, 021601(R).
Morsch, O., M. Cristiani, J. H. Müller, D. Ciampini, and E. Arimondo, 2003a, Laser Phys. **13**, 594.
Morsch, O., J. H. Müller, D. Ciampini, M. Cristiani, P. B. Blakie, C. J. Williams, P. S. Julienne, and E. Arimondo, 2003b, Phys. Rev. A **67**, 031603(R).
Morsch, O., J. H. Müller, M. Cristiani, D. Ciampini, and E. Arimondo, 2001, Phys. Rev. Lett. **87**, 140402.
Mueller, E. J., 2002, Phys. Rev. A **66**, 063603.
Niu, Q., X. G. Zhao, G. A. Georgakis, and M. G. Raizen, 1996, Phys. Rev. Lett. **76**, 4504.
Orzel, C., A. K. Tuchman, M. Fenselau, M. Yasuda, and M. Kasevich, 2001, Science **291**, 2386.
Ostrovskaya, E. A., and Y. S. Kivshar, 2003, Phys. Rev. Lett. **90**, 160407.
Ostrovskaya, E. A., and Y. S. Kivshar, 2004a, Phys. Rev. Lett. **93**, 160405.
Ostrovskaya, E. A., and Y. S. Kivshar, 2004b, Opt. Express **12**, 19.
Ott, H., E. de Mirandes, F. Ferlaino, G. Roati, G. Modugno, and M. Inguscio, 2004, Phys. Rev. Lett. **92**, 160601.
Ovchinnikov, Y. B., J. H. Müller, M. R. Doery, E. J. D. Vredenbregt, K. Helmerson, S. L. Rolston, and W. D. Phillips, 1999, Phys. Rev. Lett. **83**, 284.
Ozeri, R., N. Katz, J. Steinhauer, E. Rowen, and N. Davidson, 2003, Phys. Rev. Lett. **90**, 170401.
Ozeri, R., J. Steinhauer, N. Katz, and N. Davidson, 2002, Phys. Rev. Lett. **88**, 220401.
Paredes, B., A. Widera, V. Murg, O. Mandel, S. Fölling, I. Cirac, G. V. Shlyapnikov, T. W. Hänsch, and I. Bloch, 2004, Nature (London) **429**, 277.
Pedri, P., L. Pitaevskii, S. Stringari, C. Fort, S. Burger, F. S. Cataliotti, P. Maddaloni, F. Minardi, and M. Inguscio, 2001, Phys. Rev. Lett. **87**, 220401.
Pethick, C. J., and H. Smith, 2002, *Bose-Einstein Condensation in Dilute Gases* (Cambridge University Press, Cambridge).
Phillips, W. D., 1998, Rev. Mod. Phys. **70**, 685.
Pitaevskii, L., and S. Stringari, 2001, Phys. Rev. Lett. **87**, 180402.
Pitaevskii, L., and S. Stringari, 2003, *Bose-Einstein Condensation* (Clarendon, Oxford).
Plata, J., 2004, Phys. Rev. A **69**, 033604.
Porto, J. V., S. Rolston, B. L. Tolra, C. J. Williams, and W. D. Phillips, 2003, Philos. Trans. R. Soc. London, Ser. A **361**, 1417.
Pu, H., L. O. Baksmaty, W. Zhang, N. P. Bigelow, and P. Meystre, 2003, Phys. Rev. A **67**, 043605.
Raussendorf, R., and H. J. Briegel, 2001, Phys. Rev. Lett. **86**, 5188.
Raussendorf, R., D. E. Browne, and H. J. Briegel, 2003, Phys. Rev. A **68**, 022312.
Richard, S., F. Gerbier, J. H. Thywissen, M. Hugbart, P. Bouyer, and A. Aspect, 2003, Phys. Rev. Lett. **91**, 010405.
Roati, G., E. de Mirandes, F. Ferlaino, H. Ott, G. Modugno, and M. Inguscio, 2004, Phys. Rev. Lett. **92**, 230402.
Roth, R., and K. Burnett, 2003, Phys. Rev. A **67**, 031602(R).
Roth, R., and K. Burnett, 2004, Phys. Rev. A **69**, 021601(R).
Ruostekoski, J., G. V. Dunne, and J. Javanainen, 2002, Phys. Rev. Lett. **88**, 180401.
Russel, J. S., 1845, Report of the 14th meeting of the British Association for the Advancement of Science (unpublished), p. 311.
Salasnich, L., A. Parola, and L. Reatto, 2002, Phys. Rev. A **65**, 043614.
Santos, L., M. A. Baranov, J. I. Cirac, H.-U. Everts, H. Fehrmann, and M. Lewenstein, 2004, Phys. Rev. Lett. **93**, 030601.
Sarlo, L. D., L. Fallani, J. E. Lye, M. Modugno, R. Sears, C. Fort, and M. Inguscio, 2005, Phys. Rev. A **72**, 013603.
Scott, R. G., S. Bujkiewicz, T. M. Fromhold, P. B. Wilkinson, and F. W. Sheard, 2002, Phys. Rev. A **66**, 023407.
Scott, R. G., T. M. Martin, A. M. Fromhold, F. W. Bujkiewicz, S. Sheard, and M. Leadbeater, 2003, Phys. Rev. Lett. **90**, 110404.
Simsarian, J. E., J. Denschlag, M. Edwards, C. W. Clark, L. Deng, E. W. Hagley, K. Helmerson, S. L. Rolston, and W. D. Phillips, 2000, Phys. Rev. Lett. **85**, 2040.
Smerzi, A., S. Fantoni, S. Giovanazzi, and S. R. Shenoy, 1997, Phys. Rev. Lett. **79**, 4950.
Smerzi, A., and A. Trombettoni, 2003, Phys. Rev. A **68**, 023613.
Smerzi, A., A. Trombettoni, P. G. Kevrekidis, and A. R. Bishop, 2002, Phys. Rev. Lett. **89**, 170402.
Stamper-Kurn, D. M., A. P. Chikkatur, A. Görlitz, S. Inouye, S. Gupta, D. E. Pritchard, and W. Ketterle, 1999, Phys. Rev. Lett. **83**, 2876.
Steel, M. J., and W. Zhang, 1998, e-print cond-mat/9810284.
Steinhauer, J., N. Katz, R. Ozeri, N. Davidson, C. Tozzo, and F. Dalfovo, 2003, Phys. Rev. Lett. **90**, 060404.
Steinhauer, J., R. Ozeri, N. Katz, and N. Davidson, 2002, Phys. Rev. Lett. **88**, 120407.
Stenger, J., S. Inouye, A. P. Chikkatur, D. M. Stamper-Kurn, D. E. Pritchard, and W. Ketterle, 1999, Phys. Rev. Lett. **82**, 4569.
Stock, S., G. Hadzibabic, B. Battelier, M. Cheneau, and J. Dalibard, 2005, Phys. Rev. Lett. **95**, 190403.
Stöferle, T., H. Moritz, C. Schori, M. Köhl, and T. Esslinger, 2004, Phys. Rev. Lett. **92**, 130403.
Stringari, S., 1996, Phys. Rev. Lett. **77**, 2360.
Trombettoni, A., and A. Smerzi, 2001, Phys. Rev. Lett. **86**, 2353.
Tsukada, N., 2002, Phys. Rev. A **65**, 063608.
Vogels, J. M., K. Xu, C. Raman, J. R. Abo-Shaeer, and W. Ketterle, 2002, Phys. Rev. Lett. **88**, 060402.
Wilkens, M., E. Schumacher, and P. Meystre, 1991, Phys. Rev. A **44**, 3130.

Wu, B., R. B. Diener, and Q. Niu, 2002, Phys. Rev. A **65**, 025601.
Wu, B., and Q. Niu, 2000, Phys. Rev. A **61**, 023402.
Wu, B., and Q. Niu, 2001, Phys. Rev. A **64**, 061603(R).
Wu, B., and Q. Niu, 2002, Phys. Rev. Lett. **89**, 088901.
Wu, B., and Q. Niu, 2003, New J. Phys. **5**, 104.
Yulin, A. V., and D. V. Skryabin, 2003, Phys. Rev. A **67**, 023611.
Zener, G., 1932, Proc. R. Soc. London, Ser. A **137**, 696.
Zobay, O., S. Pötting, P. Meystre, and E. M. Wright, 1999, Phys. Rev. A **59**, 643.
Zwerger, W., 2003, J. Opt. B: Quantum Semiclassical Opt. **5**, 9.